AEDC-TR-68-193

cy #4

THEORETICAL AND EXPERIMENTAL INVESTIGATION OF BOUNDARY LAYERS IN LOW DENSITY HYPERSONIC AXISYMMETRIC NOZZLES

David L. Whitfield

ARO, Inc.

September 1968

AEROSPACE ENVIRONMENTAL FACILITY
ARNOLD ENGINEERING DEVELOPMENT CENTER
AIR FORCE SYSTEMS COMMAND
ARNOLD AIR FORCE STATION, TENNESSEE

NOTICES

When U. S. Government drawings specifications, or other data are used for any purpose other than a definitely related Government procurement operation, the Government thereby incurs no responaibility nor any obligation whatsoever, and the fact that the Government may have formulated, furnished, or in any way supplied the said drawings, apecificationa, or other data, is not to be regarded by implication or otherwise, or in any manner licenaing the holder or any other peraon or corporation, or conveying any rights or permiasion to manufacture, use, or sell any patented invention that may in any way be related thereto.

Qualified users may obtain copies of this report from the Defense Documentation Center.

References to named commercial producta in thia report are not to be conaidered in any aense aa an endorsement of the product by the United States Air Force or the Government.

THEORETICAL AND EXPERIMENTAL INVESTIGATION OF BOUNDARY LAYERS IN LOW DENSITY HYPERSONIC AXISYMMETRIC NOZZLES

David L. Whitfield
ARO, Inc.

AF—AEDC
Arnold AFS Tenn

FOREWORD

The research reported herein was sponsored by Headquarters, Arnold Engineering Development Center (AEDC), Air Force Systems Command (AFSC), Arnold Air Force Station, Tennessee, under Program Element 6240539F, Project 7663, Task 766301.

The results of research were obtained by ARO, Inc. (a subsidiary of Sverdrup & Parcel and Associates, Inc.) contract operator of AEDC, AFSC, under Contract F40600-69-C-0001. The research was performed from September 1967 to January 1968 under ARO Project No. ST8002, and the manuscript was submitted for publication on August 5, 1968.

The work reported herein was used as a thesis for partial fulfillment of the requirements for the degree of Master of Science from the University of Tennessee Space Institute. The author wishes to express his appreciation to Dr. Clark Lewis who made available a modified version of the original Jaffe, Lind, and Smith computer program from which the program used herein was obtained after further modification.

This technical report has been reviewed and is approved.

Paul L. Landry
Major, USAF
AF Representative, AEF
Directorate of Test

Roy R. Croy, Jr.
Colonel, USAF
Director of Test

ABSTRACT

The viscous flow region in low density hypersonic axisymmetric nozzles was investigated both theoretically and experimentally. Non-similar solutions were obtained for the internal laminar boundary layer equations which include second-order transverse curvature terms. These solutions were obtained on a CDC 1604 digital computer. Four existing low density axisymmetric nozzles were considered. Numerical solutions were obtained for these nozzles using various plenum chamber conditions and wall temperature distributions. The plenum chamber conditions used in the numerical solutions for these nozzles produced a test section Mach number range of about 3.0 to 18.0 and a test section Reynolds number per foot range of about 1000 to 15,000. Some results of the numerical solutions are compared with experimental measurements of pitot pressure, relative heat flux, and nozzle wall heat transfer coefficients. In all comparisons the numerical solutions appear to be consistent with the experimental data. The results of this investigation indicated that the boundary layer equations adequately described the viscous region in a nozzle where the mean free path is of the order of one-tenth of an inch; and furthermore, these equations adequately described the viscous region where the boundary layer thickness was of the order of the nozzle radius.

CONTENTS

ILLUSTRATIONS

FIGURE PAGE

FIGURE PAGE

NOMENCLATURE

C	$\rho\mu/\rho_e\mu_e$
c_p	Constant pressure specific heat
c_f	Skin friction coefficient
f	Defined in Equation 22
g	Enthalpy ratio, H/H_o
H	Local total specific enthalpy
H_o	Total specific enthalpy in plenum chamber
h	Static specific enthalpy
k	Thermal conductivity
L	Reference body length
M	Mach number
P_o	Total pressure
p	Static pressure
P'_o	Pitot pressure
Pr	Prandtl number, $\mu c_p/k$
q_w	Nozzle wall heat transfer
R	Radius of curvature of converging portion of nozzle
R_L	Longitudinal radius of curvature in meridian plane
Re_x	Reynolds number, $\rho ux/\mu$
r_E	Nozzle wall exit radius
r_o	Nozzle wall radius
r	Defined by Equation 4

T	Static temperature
T_o	Total temperature
T_o'	Total temperature behind a normal shock
T_{aw}	Adiabatic wall temperature
t	Transverse curvature term defined by Equation 31
u	Velocity component in x direction
v	Velocity component in y direction
x	Distance along nozzle wall
y	Distance normal to nozzle wall
Z	Total axial distance
z	Distance along nozzle axis
α	Nozzle wall angle
β	Dimensionless velocity gradient, see Equation 27
δ	Boundary layer thickness defined as value of y where $u/u_e = 0.995$
δ^*	Displacement thickness
ξ	y/δ
η	Transformed y coordinate
θ	Momentum thickness
λ	Heat transfer coefficient defined by Equation 55
μ	Viscosity
ξ	Transformed x coordinate
ρ	Mass density
ψ	Stream function

Subscripts

$\mathfrak{C}$	Nozzle centerline
e	Edge of isentropic core
w	Nozzle wall

SECTION I
INTRODUCTION

Since the advent of flying vehicles there has existed the need to simulate for aerodynamic testing purposes the environment in which these vehicles travel. With the recent reality of vehicles traveling in the upper atmosphere of earth, and possibly other planets, this need has become more important due to the complication of problems associated with an unfamiliar environment.

The flow field about a vehicle moving in the earth's atmosphere at altitudes of about 200,000 feet to 400,000 feet, is characterized by low Reynolds number and usually high Mach number. As is well known, when the Reynolds number is low the boundary layer is laminar and thick. Therefore, an inherent problem in the design of a nozzle for a wind tunnel which is to simulate this flow regime is the analysis of thick laminar boundary layers. This can be exemplified by considering an existing low density Mach ten nozzle, which will be discussed later, that has been used to take much useful aerodynamic data. The boundary layer thickness is about 80 per cent of the nozzle radius which means that 96 per cent of the actual area of the nozzle is dominated by viscous effects. The necessity of investigating boundary layers in low density hypersonic nozzles is, therefore, rather obvious.

The purpose of this investigation is to theoretically study the viscous flow field associated with low density hypersonic

axisymmetric nozzles, and to compare experimental data with the results of the theoretical solutions.

The approach taken here is to obtain general non-similar solutions to an appropriate set of boundary layer equations which contain second-order transverse curvature terms. These equations are transformed into the $\xi\eta$-plane for convenience of numerical solution. A general discussion of the procedure used to obtain the numerical solutions is given. Solutions for various conditions in four low density nozzles will be presented, followed by a comparison of theoretical results and experimental data.

Three of the four nozzles considered use arc heaters to generate high enthalpy conditions in the plenum chamber. These high enthalpy conditions force one to investigate the possibility of ionization and dissociation due to the high temperatures produced by the arc. Since nitrogen is the test gas used in each nozzle, it is possible to use a plenum chamber which is sufficiently large to permit recombination and also sufficiently small to prevent an unreasonable amount of energy loss due to heat transfer. The analysis is therefore simplified since the specie concentration equations do not have to be included in the governing system of equations.

The design of low density hypersonic nozzles is usually accomplished by applying a boundary layer correction to some desired inviscid flow. One such method is due to Potter and Durand (1) , which

was recently modified by Potter and Carden (2). This method is based on an integral technique which uses the similar solutions of Cohen and Reshotko (3). The results given by this method have proved to be very useful in designing a nozzle for a particular test condition. On the subject of non-similar internal laminar boundary layers the literature appears to be rather limited. To the author's knowledge there presently exist no non-similar solutions to the internal laminar boundary layer equations for a specified nozzle geometry. This situation is somewhat unfortunate since it is desirable from both the practical and economic point of view to be able to determine what flow conditions might be expected from one nozzle. Similar solutions are not applicable for such an investigation since similarity cannot be satisfied in general for specified plenum chamber conditions, nozzle geometry, and wall temperature distribution all occurring simultaneously. The present work was undertaken in order to provide a means of analyzing nozzles without the restriction of similar boundary layers.

SECTION II
MATHEMATICAL ANALYSIS

In order to take maximum advantage of the integration techniques developed by Jaffe, Lind, and Smith (4), the mathematical formulation of this internal flow problem is handled similarly to their work for external flow. The governing system of equations is transformed from the physical xy-plane into a $\xi\eta$-plane by appropriate transformation of variables. Certain boundary layer parameters are derived and the numerical solution of the transformed equations is discussed.

2.1 GOVERNING SYSTEM OF EQUATIONS

The governing equations are taken from Probstein and Elliott (5). These equations in curvilinear coordinates including second-order transverse curvature terms are:

continuity equation

$$\frac{\partial(\rho r u)}{\partial x} + \frac{\partial(\rho r v)}{\partial y} = 0 \tag{1}$$

momentum equation

$$\rho u \frac{\partial u}{\partial x} + \rho v \frac{\partial u}{\partial y} = - \frac{dp}{dx} + \frac{1}{r} \frac{\partial}{\partial y} \left(\ddot{r}\mu \frac{\partial u}{\partial y} \right) \tag{2}$$

static energy equation

$$\rho u \frac{\partial h}{\partial x} + \rho v \frac{\partial h}{\partial y} = u \frac{dp}{dx} + \frac{1}{r} \frac{\partial}{\partial y} \left(r \frac{\mu}{Pr} \frac{\partial h}{\partial y} \right) + \mu \left(\frac{\partial u}{\partial y} \right)^2 \tag{3}$$

The coordinate system is defined in Figure 1 with the r(x,y) term being defined for internal flow as

$$r(x,y) = r_o(x) - y \cos \alpha \tag{4}$$

Probstein and Elliott obtained Equations 1, 2, and 3 by the usual order of magnitude analysis of the general form of the continuity equation, Navier-Stokes equations, and energy equation expressed in curvilinear coordinates. The assumptions made in the analysis were that δ/R_L is small compared to unity and δ/r_o is of the order of unity. Since the boundary layer thickness may be of the order of the nozzle radius, Equations 1, 2, and 3 are valid for nozzles which have a longitudinal radius of curvature, R_L, much larger than the nozzle radius, r_o. This stipulation is normally satisfied in axisymmetric nozzles which are used in low density wind tunnels.

The axisymmetric boundary layer equations, which contain second-order transverse curvature terms, can be obtained from Equations 1, 2, and 3 by replacing r with r_o. Since r_o is a function of x only, it is eliminated from Equations 2 and 3 and therefore only appears in the continuity equation. The resulting axisymmetric equations can be used to describe internal or external boundary layers.

Equations 1, 2, and 3 differ slightly from the corresponding equations of Probstein and Elliott in that the specific heat and Prandtl

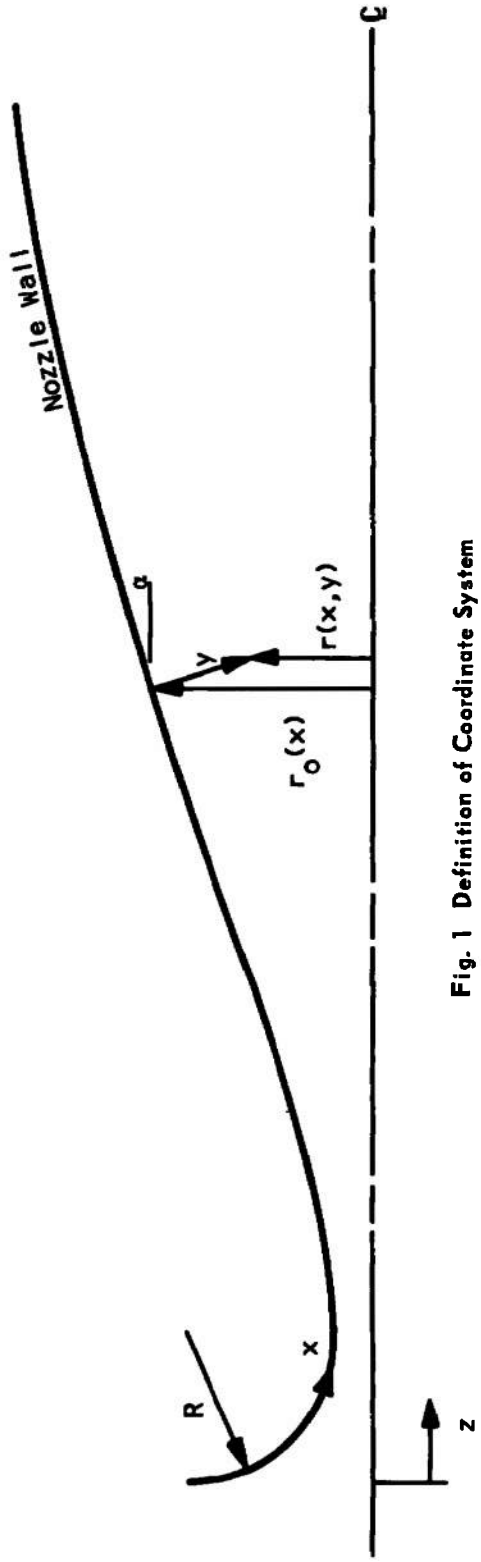

Fig. 1 Definition of Coordinate System

number are not necessarily assumed to be constants. However, all numerical results presented herein are for constant Prandtl number and constant specific heat.

A more convenient form of the energy equation for this work is the total energy equation. It is derived by multiplying the momentum equation by u and adding the result to the static energy equation to give

$$\rho u \frac{\partial H}{\partial x} + \rho v \frac{\partial H}{\partial y} = \frac{1}{r} \frac{\partial}{\partial y} \left\{ r \left[\frac{\mu}{Pr} \frac{\partial H}{\partial y} + \mu \left(1 - \frac{1}{Pr} \right) u \frac{\partial u}{\partial y} \right] \right\} \tag{5}$$

where

$$H = h + \frac{u^2}{2} \tag{6}$$

As noted by the total derivative of p with respect to x in Equations 2 and 3, the y component of the momentum equation is given by

$$- \frac{\partial p}{\partial y} = 0 \tag{7}$$

The validity of this equation is sometimes questioned for very thick laminar boundary layers. However, the analysis of Probstein and Elliott indicates that this equation is consistent with the other equations in the governing set. Also, the numerical solutions of the governing equations, which implicitly contain Equation 7, are consistent with experimental data.

Expressing μ as an arbitrary function of T

$$\mu = \mu(T) \tag{8}$$

and taking the thermal equation of state as

$$p = \rho RT \tag{9}$$

one has, with Equations 1, 2, and 5 and the appropriate boundary conditions, the governing system of equations whose solution is desired.

For the boundary conditions at the edge of the boundary layer, it is assumed that an isentropic core flow exists along the centerline of the nozzle. There is no restriction on the size of this core, as long as the gas properties along the centerline can be found from the isentropic flow relations. The boundary conditions at the nozzle wall are taken as zero velocity and a prescribed wall temperature distribution. A specified wall heat transfer distribution could be used in place of the wall temperature distribution; however, the boundary condition used herein is the latter.

2.2 TRANSFORMATION OF THE GOVERNING EQUATIONS

2.2.1 Transformation Variables

The transformation variables used are a combination of a modified form of the Mangler transformation proposed by Probstein and Elliott, and the Illingworth transformation sometimes referred to as the Illingworth-Levy transformation.

In the Mangler transformation the assumption is made that $\delta << r_o(x)$ and hence $r(x,y)$ is approximately equal to $r_o(x)$. However, for boundary layer thicknesses of the order of $r_o(x)$, this approximation is not justified. In this light Probstein and Elliott used the

following transformation to transform the axisymmetric boundary layer equations containing second-order transverse curvature terms to an almost two-dimensional form in the independent variables $\bar{x}$ and $\bar{y}$

$$d\bar{x} = \frac{r_o^2(x)}{L^2}\, dx \tag{10}$$

$$d\bar{y} = \frac{r(x,y)}{L}\, dy \tag{11}$$

This transformation differs from Mangler's original transformation in that $r(x,y)$ is used to replace $r_o(x)$ in the change of the independent variable y.

In working with the boundary layer equations in two-dimensional form, Illingworth (6) used a transformation that has been expressed by Levy (7) in the following form

$$M = \int_o^{\bar{x}} \mu_e \rho_e u_e\, d\bar{x} \tag{12}$$

$$N = \frac{\rho_e u_e}{\sqrt{2M}} \int_o^{\bar{y}} \frac{\rho}{\rho_e}\, d\bar{y} \tag{13}$$

Combining Equations 10 and 11 with Equations 12 and 13, redefining the limits of integration, and introducing two new variables ξ and η to replace M and N, yield the following transformation variables

$$\xi = \int_o^{x} \mu_e \rho_e u_e \frac{r_o^2}{L^2}\, dx \tag{14}$$

$$\eta = \frac{\rho_e u_e}{\sqrt{2\xi}} \int_0^y \frac{\rho}{\rho_e} \frac{r}{L} \, dy \tag{15}$$

It might be pointed out that the transformations can be carried out without introducing the characteristic length L.

2.2.2 Transformed Equations

Applying the chain rule of partial differentiation to the transformation variables, the necessary operators become

$$\left(\frac{\partial}{\partial y}\right)_x = \frac{u_e \rho}{\sqrt{2\xi}} \frac{r}{L} \left(\frac{\partial}{\partial \eta}\right)_\xi \tag{16}$$

$$\left(\frac{\partial}{\partial x}\right)_y = \frac{\rho_e u_e \mu_e r_o^2}{L^2} \left[\left(\frac{\partial}{\partial \xi}\right)_\eta + \left(\frac{\partial \eta}{\partial \xi}\right)_y \left(\frac{\partial}{\partial \eta}\right)_\xi\right] \tag{17}$$

Although the term $\left(\frac{\partial \eta}{\partial \xi}\right)_y$ does not appear in the final equations, it is included here for completeness

$$\left(\frac{\partial \eta}{\partial \xi}\right)_y = \frac{u_e}{\sqrt{2\xi}} \int_0^y \frac{1}{L} \frac{\partial(\rho r)}{\partial \xi} \, dy + \left(\frac{du_e}{d\xi} - \frac{u_e}{2\xi}\right) \int_0^y \frac{\rho r}{L\sqrt{2\xi}} \, dy \tag{18}$$

The continuity equation is identically satisfied by introducing the stream function ψ

$$\rho r u = \frac{\partial \psi}{\partial y} \tag{19}$$

$$\rho r v = - \frac{\partial \psi}{\partial x} \tag{20}$$

Applying the operator given by Equation 16 to Equation 19 gives

$$\left(\frac{\partial \psi}{\partial \eta}\right)_{\xi} = \sqrt{2\xi}\, L\, \frac{u}{u_e} \tag{21}$$

Defining a non-dimensional stream function $f(\xi,\eta)$ by

$$\psi(\xi,\eta) = \sqrt{2\xi}\; L\, f(\xi,\eta) \tag{22}$$

one has

$$\frac{u}{u_e} = f'(\xi,\eta) \tag{23}$$

where the prime denotes differentiation with respect to η.

Substituting the steady flow Euler's equation

$$\frac{dp}{dx} = - \rho_e u_e \frac{du_e}{dx} \tag{24}$$

into the momentum equation and applying the operators given by Equations 16 and 17 to Equations 2 and 5, yield the following forms of the momentum and energy equations

$$\left(\frac{r^2}{r_o^2}\, Cf''\right)' + \beta\left(\frac{\rho_e}{\rho} - f'^2\right) + ff'' = 2\xi \left(f' \frac{\partial f'}{\partial \xi} - f'' \frac{\partial f}{\partial \xi}\right) \tag{25}$$

$$\left\{\frac{r^2}{r_o^2}\, C\left[\frac{g'}{Pr} + \frac{u_e^2}{H_o}\left(1 - \frac{1}{Pr}\right) f'f''\right]\right\}' + fg' = 2\xi \left(f' \frac{\partial g}{\partial \xi} - g' \frac{\partial f}{\partial \xi}\right) \tag{26}$$

where

$$\beta = \frac{2\xi}{u_e} \frac{du_e}{d\xi} \tag{27}$$

$$C = \frac{\rho\mu}{\rho_e \mu_e} \tag{28}$$

$$g = \frac{H}{H_o} \tag{29}$$

It is of interest here to consider the term r^2/r_o^2 in Equations 25 and 26. If the approximation $r = r_o$ is made, as for thin boundary layers, the term r^2/r_o^2 is one and the resulting equations describe boundary layers without second-order transverse curvature. For this case the transformation given by Equation 15 must contain r_o rather than r. These equations can also be used to describe two-dimensional boundary layers by setting r^2/r_o^2 equal to one in Equations 25 and 26. For this case the transformations given by Equations 14 and 15 must have r_o^2/L^2 and r/L set equal to one. Hence, it would be convenient to incorporate into one program the capability of handling two-dimensional or axisymmetric boundary layers with or without second-order transverse curvature terms. This is, in fact, what Jaffe, Lind, and Smith have done.

The term r^2/r_o^2 can be written in terms of the variables ξ and η as

$$\frac{r^2}{r_o^2} = 1 - \frac{2L\sqrt{2\xi}\cos\alpha}{r_o^2 \rho_e u_e} \int_o^\eta \frac{\rho_e}{\rho} d\eta \tag{30}$$

Defining

$$t \equiv \frac{2L\sqrt{2\xi}\cos\alpha}{r_o^2\,\rho_e\,u_e}\int_o^\eta \frac{\rho_e}{\rho}\,d\eta \tag{31}$$

one can see from the discussion above that the effects of transverse curvature depend upon the parameter t. Equations 25 and 26 now become

$$\left[C(1-t)f''\right]' + \beta\left(\frac{\rho_e}{\rho} - f'^2\right) + ff'' = 2\xi\left(f'\frac{\partial f'}{\partial \xi} - f''\frac{\partial f}{\partial \xi}\right) \tag{32}$$

$$\left\{C(1-t)\left[\frac{g'}{Pr} + \frac{u_e^2}{H_o}\left(1 - \frac{1}{Pr}\right)f'f''\right]\right\}' + fg' = 2\xi\left(f'\frac{\partial g}{\partial \xi} - g'\frac{\partial f}{\partial \xi}\right) \tag{33}$$

with the boundary conditions

at $\eta = 0$

$$f = 0 \tag{34a}$$

$$f' = 0 \tag{34b}$$

$$g = g_w \tag{34c}$$

as $\eta \to \eta_e$

$$f' \to 1 \tag{34d}$$

$$g \to 1 \tag{34e}$$

2.2.3 Inverse Transformations

The inverse transformation of mapping points in the $\xi\eta$-plane back into the physical xy-plane usually does not pose a difficult

problem, especially for external flow. However, for internal flow, one should determine whether the inverse transformation exists and is one-to-one.

An existence theorem for inverse transformations, as taken from Olmsted (8), states that if: (i) ξ and η are single valued functions, (ii) ξ and η are continuously differentiable in a neighborhood of the point (c,d), and (iii) the Jacobian $J = \frac{\partial(\xi,\eta)}{\partial(x,y)}$ is nonzero at (c,d), then there exists a neighborhood about the image of the point (c,d) such that the inverse transformation is assured and the correspondence of the points about (c,d) and their image in the xy-plane is one-to-one. For the transformation variables given by Equations 14 and 15, the only difficulty that might occur is due to the Jacobian J. From the definition of the Jacobian one finds

$$J = \frac{\mu_e \rho_e u_e^2 \rho \; r_o^2 r}{L^3} \tag{35}$$

There are two places where the Jacobian is zero. One is in the plenum chamber of the nozzle where $u_e = 0$. This point will be discussed in the section on the Solution of the Transformed Equations. The other is along the centerline of the nozzle where $r \equiv 0$. This point could obviously be avoided by not integrating quite all the way to the centerline; but, in the numerical solution of this problem no difficulties were encountered in obtaining inverse transformations at the nozzle centerline. Even though the singularity posed no problem in this work,

the point to be made is that in working with internal flows, the centerline may pose certain problems that require special attention. This can be seen, for example, in the work of Adams (9).

Only the inverse transformation of η is necessary here since ξ is calculated for each prescribed value of x. The inverse of Equation 15 is given by

$$y = \frac{\sqrt{2\xi}}{\rho_e u_e} \int_0^\eta \frac{\rho_e}{\rho} \frac{L}{r} \, d\eta + \Omega(\xi) \tag{36}$$

Applying the condition that $y = 0$ at $\eta = 0$ gives $\Omega(\xi) \equiv 0$ and hence

$$y = \frac{\sqrt{2\xi}}{\rho_e u_e} \int_0^\eta \frac{\rho_e}{\rho} \frac{L}{r} \, d\eta \tag{37}$$

2.3 BOUNDARY LAYER PARAMETERS

Certain parameters which are convenient in describing the effects produced by boundary layers are the displacement thickness, momentum thickness, skin friction, heat transfer, and Stanton number. For calculation purposes these quantities are expressed in terms of the transformation variables ξ and η.

The displacement thickness, δ^*, which is a measure of mass-flow defect, is defined by

$$\int_0^{\delta^*} 2\pi \, r \, \rho_e u_e \, dy = \int_0^{y_e} 2\pi r \, (\rho_e \, u_e - \rho u) \, dy \tag{38}$$

which takes into account transverse curvature. The upper limit of integration in the right hand side of this equation indicates the distance from the wall that the numerical integration has been carried to satisfy, within prescribed accuracy, the boundary condition $u/u_e \to 1$. By substituting Equation 4 into Equation 38, the left hand side of this equation can be integrated in closed form yielding a quadratic expression for δ^*. The two solutions for δ^* give one value less than r_o and one greater than r_o. Of course, the one applicable to internal flow is δ^* less than r_o. Using Equation 37 to express the result in the transformed plane gives

$$\delta^* = \frac{r_o}{\cos \alpha} \left\{ 1 - \left[1 - \frac{2L \sqrt{2\xi} \cos \alpha}{r_o^2 \rho_e u_e} \int_o^{\eta_e} \left(\frac{\rho_e}{\rho} - f' \right) d\eta \right]^{\frac{1}{2}} \right\} \quad (39)$$

where η_e is the value of η required to satisfy, within prescribed accuracy, the boundary condition $u/u_e \to 1$.

The momentum thickness, θ, which is a measure of momentum-flow defect, is defined by

$$\int_o^{\theta} 2\pi r \rho_e u_e^2 \, dy = \int_o^{Y_e} 2\pi r \rho (u_e u - u^2) \, dy \quad (40)$$

Treating this similarly to δ^* yields

$$\theta = \frac{r_o}{\cos \alpha} \left\{ 1 - \left[1 - \frac{2L \sqrt{2\xi} \cos \alpha}{r_o^2 \rho_e u_e} \int_o^{\eta_o} f'(1-f') d\eta \right]^{\frac{1}{2}} \right\} \quad (41)$$

The skin friction coefficient is defined by

$$c_f = \frac{\tau_w}{\frac{1}{2} \rho_e u_e^2} \tag{42}$$

where the shear stress τ_w is

$$\tau_w = \mu_w \left(\frac{\partial u}{\partial y}\right)_w \tag{43}$$

Applying the operator given by Equation 16, evaluated at the wall, to τ_w gives the following result for c_f

$$c_f = \left(\frac{2}{\xi}\right)^{\frac{1}{2}} \frac{r_o}{L} \frac{\rho_w}{\rho_e} \mu_w f''_w \tag{44}$$

The heat transfer at the wall is given by

$$-q_w = k \left(\frac{\partial T}{\partial y}\right)_w \tag{45}$$

Treating this similarly to c_f yields

$$- q_w = \frac{\mu_w \rho_w H_o u_e r_o g'_w}{Pr_w \sqrt{2\xi} L} \tag{46}$$

The Stanton number is defined as

$$St = \frac{-q_w}{\rho_e u_e H_o (1-g_w)} \tag{47}$$

which in the transformed plane is

$$St = \frac{\mu_w \rho_w r_o g'_w}{Pr_w L \rho_e \sqrt{2\xi} (1-g_w)} \tag{48}$$

Equation 37 can be used to obtain y in the form

$$y = \frac{r_o}{\cos \alpha} \left[1 - (1 - t)^{\frac{1}{2}} \right] \tag{49}$$

where t is the transverse curvature term defined by Equation 31.

2.4 SOLUTION OF THE TRANSFORMED EQUATIONS

A discussion of the numerical integration techniques used to solve the momentum and energy equations for external flow can be found in Reference 4. Hence, attention here will be focused on the application of these techniques to internal flow.

The nozzle wall radius r_o is known for each point z along the axis from the nozzle geometry. However, the coordinate system requires r_o to be known for each point x along the wall. By using the integral form of arc length one can write

$$x(z) = \int_o^z \sqrt{1 + \left(\frac{dr_o}{dz}\right)^2} \, dz \tag{50}$$

If the nozzle geometry is simple, for example a conical nozzle with the converging portion described by an arc of a circle, Equation 50 can be integrated in closed form and the inverse taken to give

$$z = A(x) \tag{51}$$

Then z can be substituted into the known expression

$$r_o = B(z) \tag{52}$$

to give

$$r_o = B[A(x)] = r_o(x) \tag{53}$$

If the nozzle wall cannot be expressed accurately by simple functions which permit integration in closed form, one must resort to numerical integration and tabulate r_o for various x values.

The solutions are started at the entrance of the converging portion of the nozzle where u_e is zero. The total conditions in the plenum chamber are therefore the initial conditions. As pointed out previously, one has a problem at the start in obtaining y since $u_e = 0$. Recalling the expression for y given by Equation 49, one notices that it contains the transverse curvature term t. The wall slope is undefined at this point, and t is zero. Therefore, Equation 49 gives $y \equiv 0$. This problem is alleviated by using the second station values of ξ and u_e in the expression for t, Equation 31.

The solution at the first station is obtained by assuming a linear temperature distribution. Also, all the derivatives in the transformed streamwise direction are taken as zero for the first station.

The basic inputs to the program are the total pressure, total enthalpy, wall temperature distribution, nozzle geometry, Prandtl number, and some initial estimated pressure distribution along the axis. Since a given nozzle will establish its own pressure distribution for each set of plenum chamber conditions, this pressure distribution must be obtained as part of the solution. This is accomplished by iteration in the following way. From the displacement thickness calculated at

each station an effective inviscid area is calculated using the corresponding wall radius. Taking the ratio of this area to the throat area a new pressure is calculated at each station from one-dimensional expansion theory. The resulting pressure distribution is then used as input to the program and the process is repeated until the pressure distribution converges within prescribed accuracy. As shown later, the solutions have converged after two or three iterations.

It should be pointed out that the throat area used to calculate the pressure distribution upstream of the throat is given by the actual geometric throat area for the first iteration, and then by the effective inviscid throat area calculated from the previous iteration for each successive iteration. All pressure distribution calculations downstream of the throat use the effective inviscid throat area corresponding to the particular iteration.

All the solutions calculated were for nitrogen since it was the test gas used in the particular nozzles considered. In order to compare some of the solutions with experimental data, the initial conditions used correspond to actual plenum chamber conditions.

The expression taken for viscosity in all the calculations was Sutherland's Law, and the Prandtl number used was Pr = 0.7068.

SECTION III
RESULTS OF CALCULATIONS

Various solutions were obtained for four different nozzles which are in operation in low density test facilities at the Arnold Engineering Development Center (AEDC). The solutions were obtained on a CDC 1604 computer in the von Kármán Facility at AEDC. The dimensions of the nozzles are given in Table I.

TABLE I
NOZZLE DIMENSIONS

Nozzle	L[a]	r*	Z	r_E	R	Type
Mach Three	67.40[b]	5.333	64.00	15.00	4.425	Conical
Mach Nine	17.34	.07343	16.59	2.407	1.0	Contoured
Mach Ten	19.62	.07405	18.67	3.833	1.0	Contoured
Mach Eighteen	59.80	.100	57.40	14.01	1.185	Conical

[a]Terms are defined in the nomenclature

[b]All dimensions are in inches

3.1 SOLUTIONS FOR MACH THREE NOZZLE

The Mach three nozzle is a 9.35° half-angle conical nozzle which operates in the ARC 8V Vacuum Chamber in the Aerospace Environmental Facility at AEDC. The nozzle wall is cooled with liquid nitrogen

at a temperature of 77°K, to reduce the boundary layer growth. Due to the cold wall, this nozzle can be operated at various plenum chamber conditions without the boundary layer merging. The plenum chamber temperatures range from 290°K to 1000°K and the plenum chamber pressures range from 100 to 1500 microns of mercury. These conditions permit a Mach number range of 2.7 to 3.5 and a Reynolds number per foot range of 100 to 3600. Solutions were obtained for plenum chamber conditions of 300°K and 500 microns of mercury with four different wall temperature distributions.

Figure 2 indicates the convergence of the solutions to a certain displacement thickness. Each iteration represents a new solution using the pressure distribution given by the previous iteration. This solution was obtained using the actual nozzle wall temperature distribution which is denoted as T_w = VI. Wall temperature distributions used for the Mach three nozzle solutions are given in Figure 3.

The effect of wall cooling is shown in Figure 4 by the results of the constant wall temperature solutions of 100°K and 200°K. The displacement thickness is more influenced by cooling than is the boundary layer thickness. This significant reduction in displacement thickness is due to the higher gas density near the wall.

Based on the indicated effects of wall cooling in Figure 4, solutions were obtained to investigate the advantage or disadvantage of cooling the nozzle exit region more thoroughly. The nozzle is presently cooled upstream of the throat by liquid nitrogen in contact with the wall, and downstream of the throat by liquid nitrogen pumped through

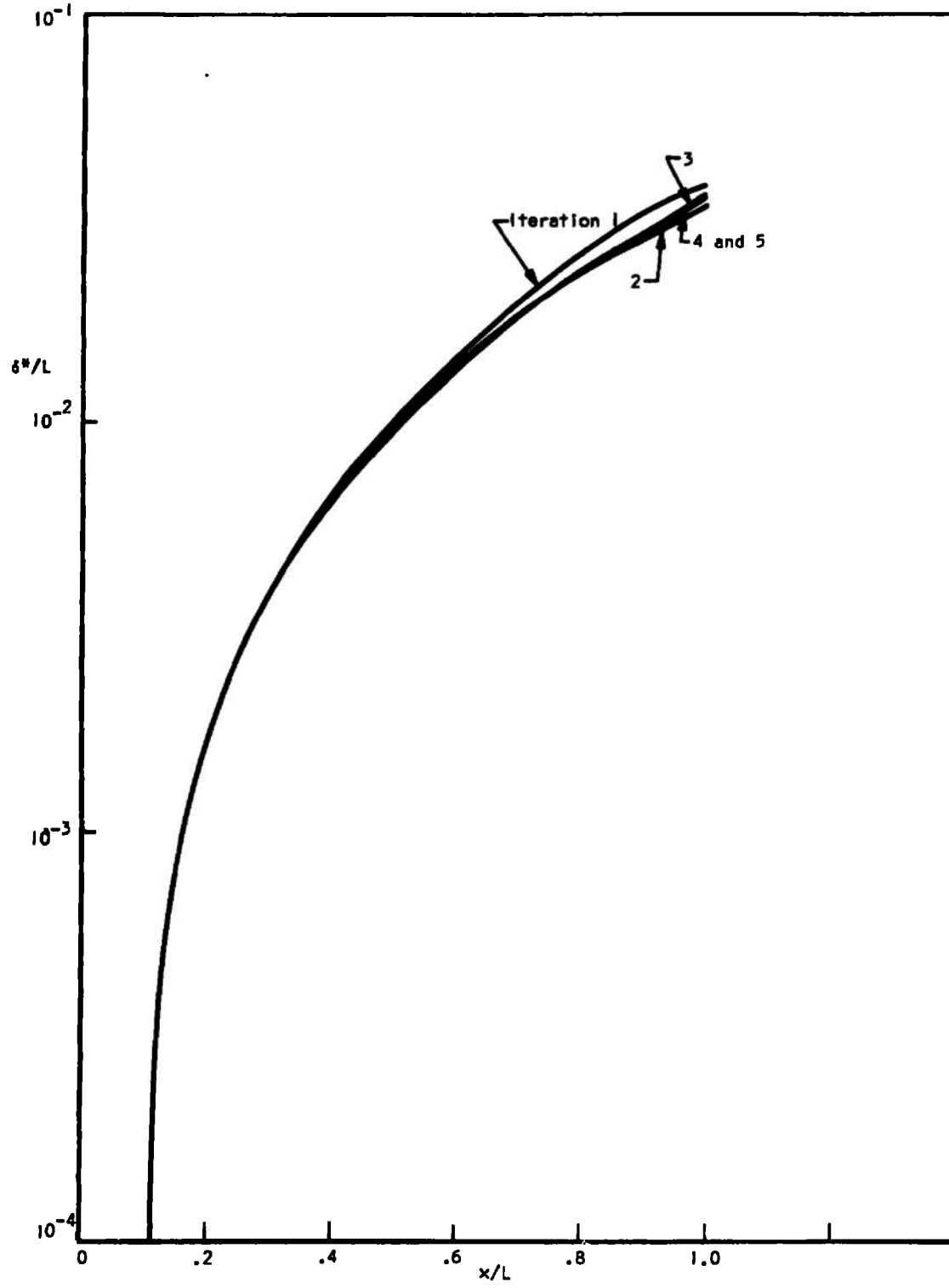

Fig. 2 Plot of Displacement Thickness for Seccessive Iterations

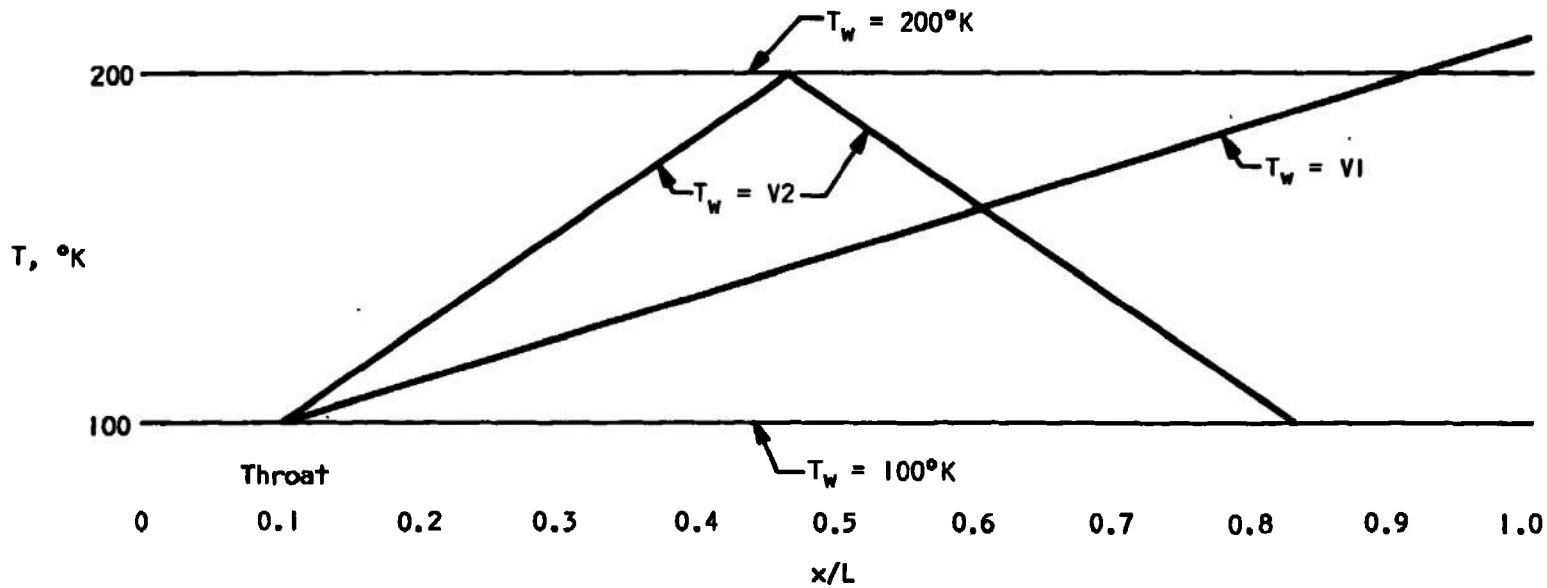

Fig. 3 Definitions of Wall Temperature Distributions Used for Mach Three Nozzle

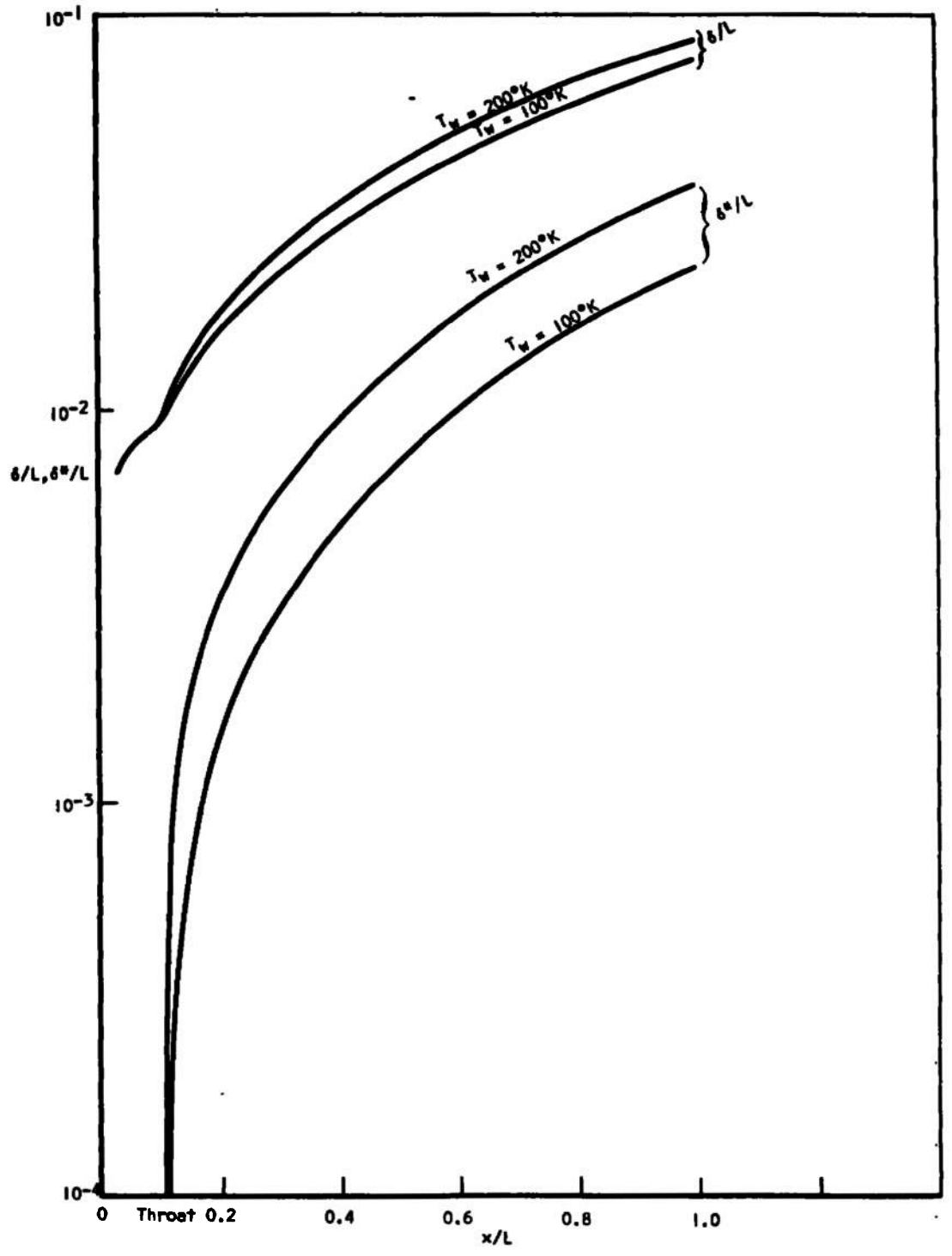

Fig. 4 Plot of Displacement Thickness and Boundary Layer Thickness for Two Different Wall Temperatures for Mach Three Nozzle

copper tubing which is wrapped around the nozzle wall. From thermocouple measurements taken along the nozzle wall the actual temperature distribution is given by T_w = V1. It is anticipated that if the last 12 inches of the nozzle were cooled by direct contact with liquid nitrogen, the resulting wall temperature distribution would be as shown by T_w = V2 of Figure 3, page 24.

The Mach number distributions along the nozzle axis for the two wall temperature distributions, V1 and V2, are given in Figure 5. The Mach number at the exit of the nozzle is increased by the T_w = V2 distribution from 3.29 to 3.40. This produces a decrease in Reynolds number per foot from 1324 to 1225. However, the axial Mach number gradient is increased at the exit plane as shown in Figure 5. It might be that neither the T_w = V1 nor T_w = V2 case provides a flow sufficiently free of axial gradients for some test purposes. In this light it might be desirable to control the wall temperature in order to produce a displacement thickness distribution that will eliminate axial gradients in the test region.

The results of the solutions for various wall temperature distributions are compared in Figures 6 through 13. In Figure 6 the velocity distribution for T_w = V2 was not sufficiently different from that for T_w = 100°K to warrant a separate curve. The boundary layer thickness appears to be about the same at the exit whether the nozzle is cooled all the way, or only in the region of the converging section and the exit. Of course the problem of axial gradients exists as previously pointed out.

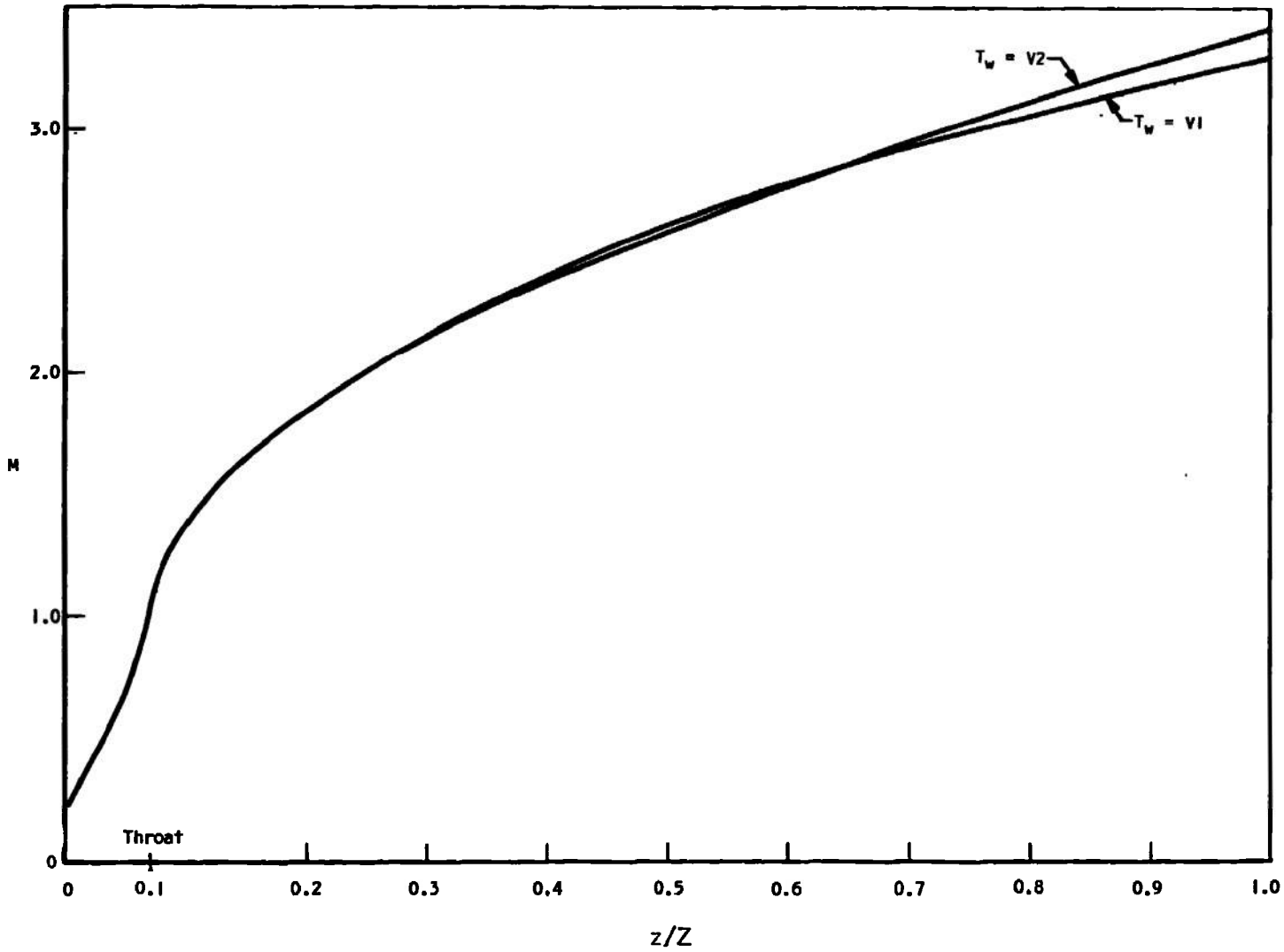

Fig. 5 Axial Mach Number Distributions for Mach Three Nozzle

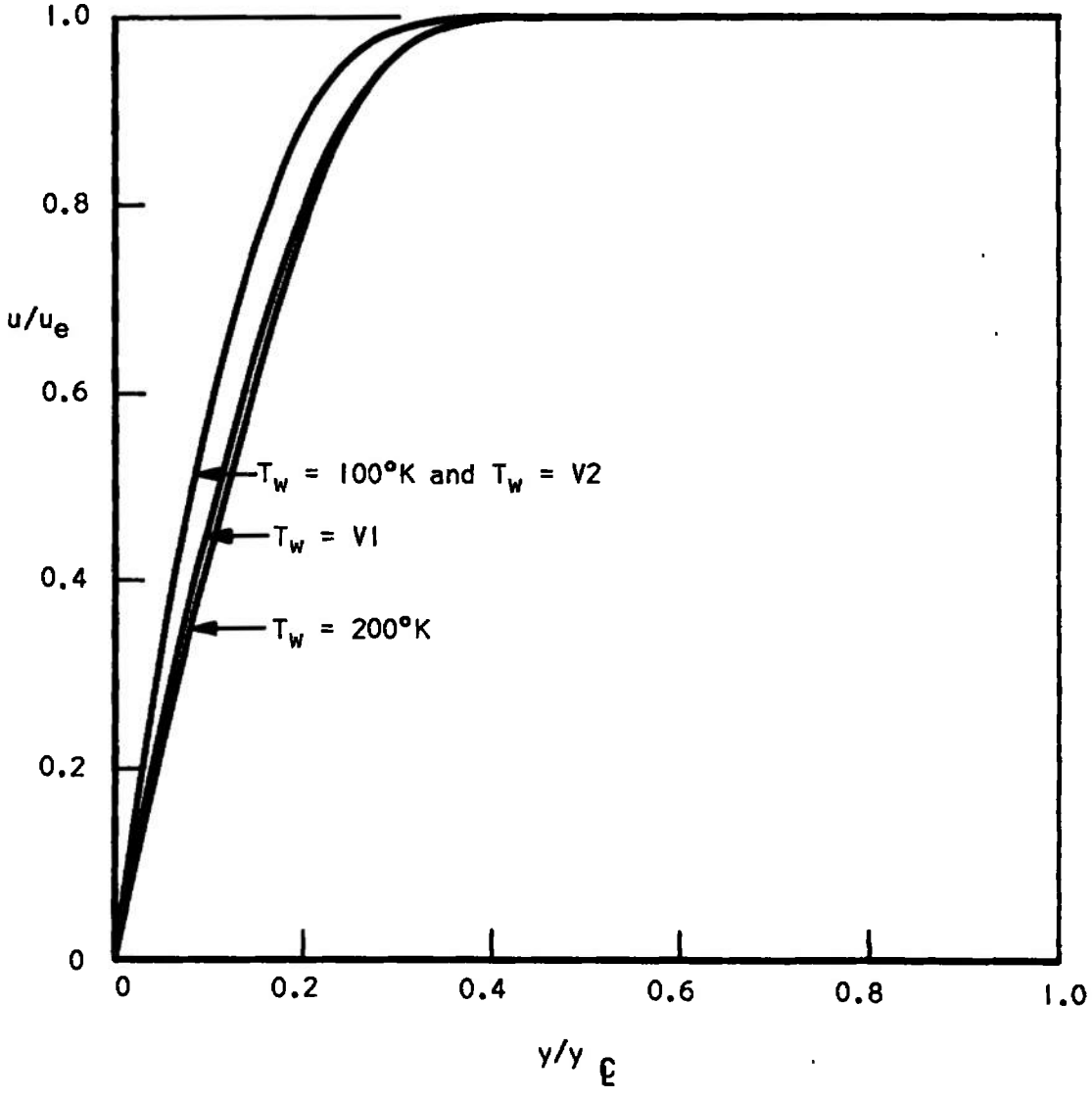

Fig. 6 Plot of Velocity Distributions at Mach Three Nozzle Exit

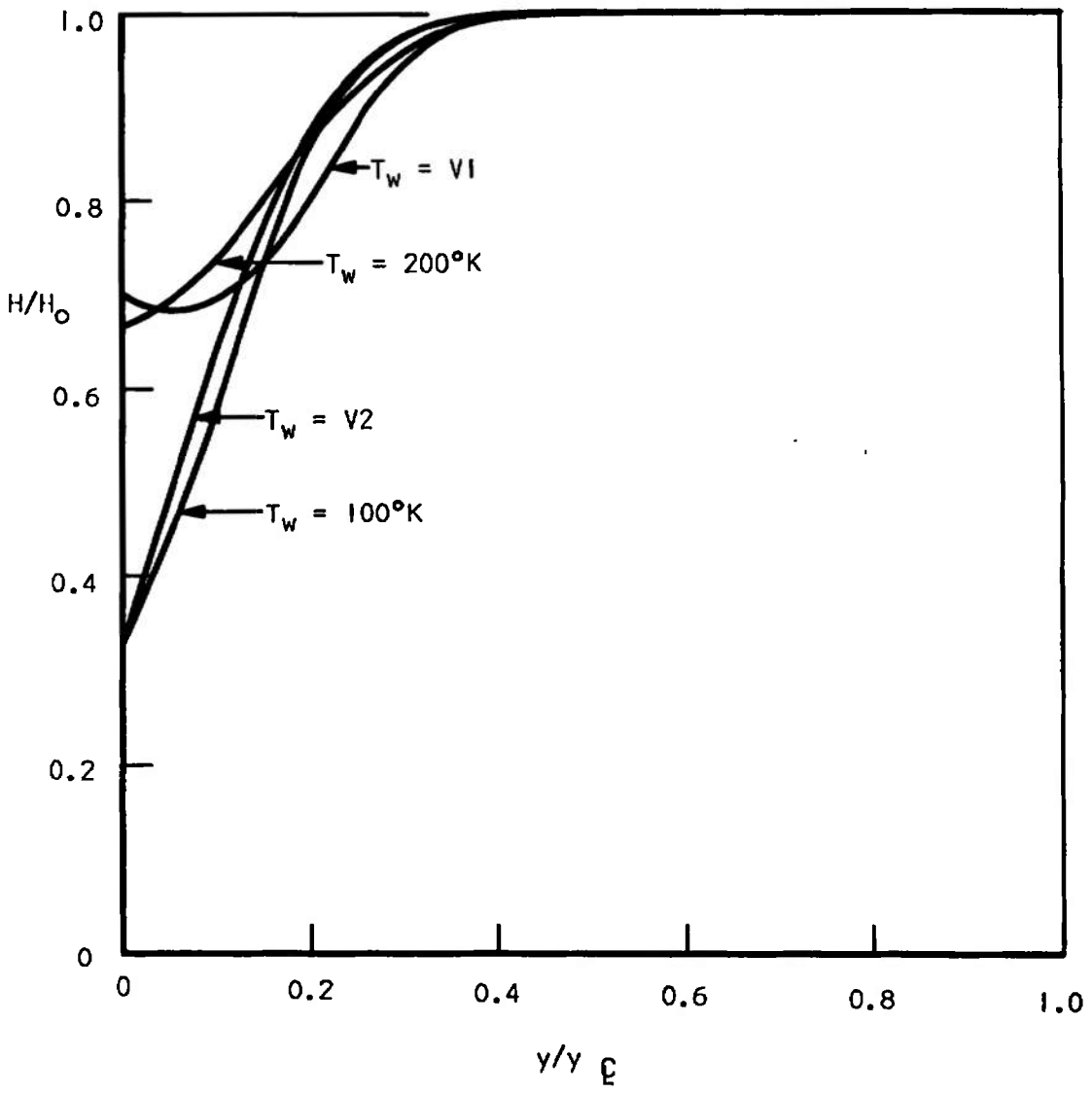

Fig. 7 Plot of Total Enthalpy Distributions at Mach Three Nozzle Exit

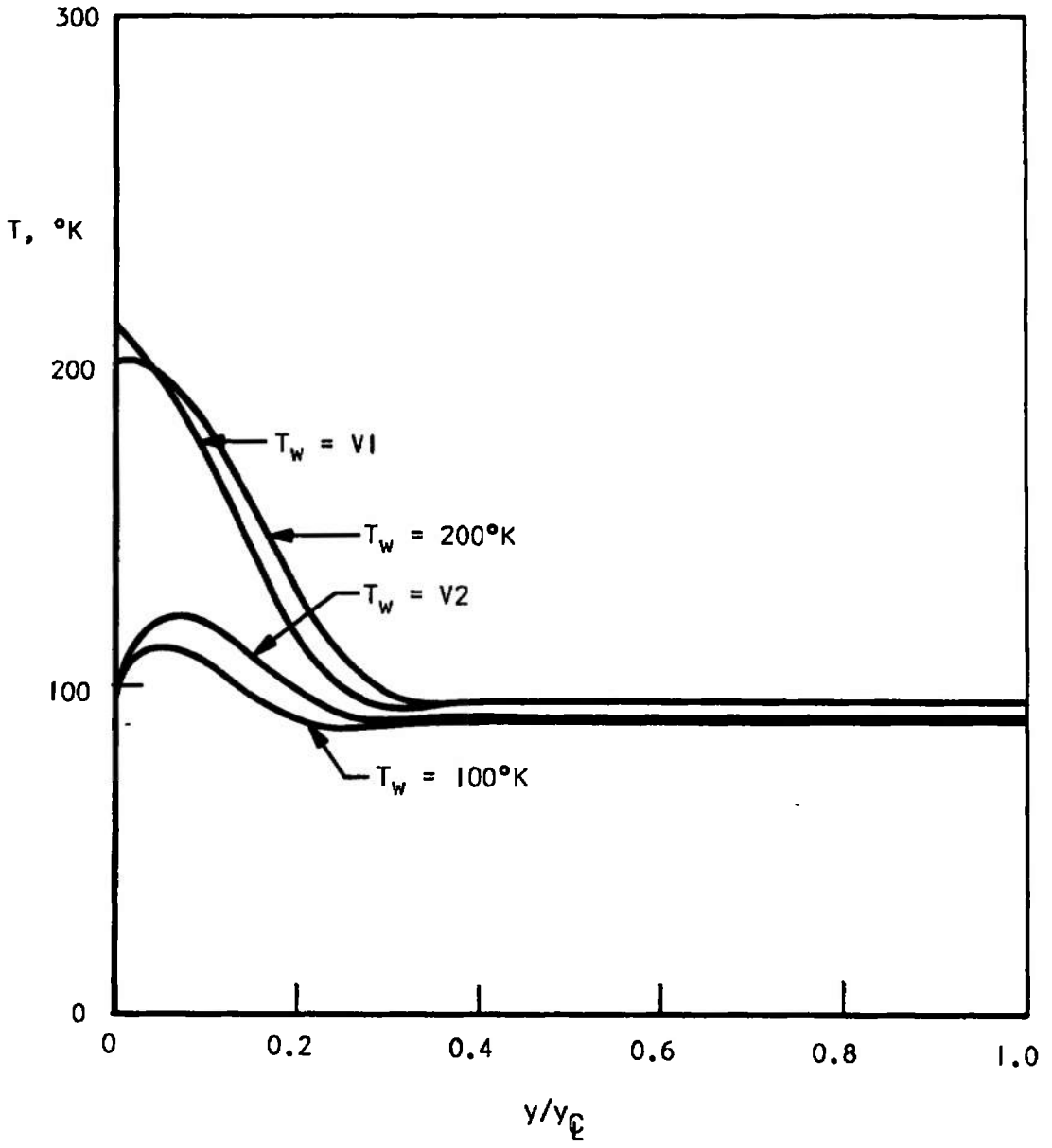

Fig. 8 Plot of Static Temperature Distributions at Mach Three Nozzle Exit

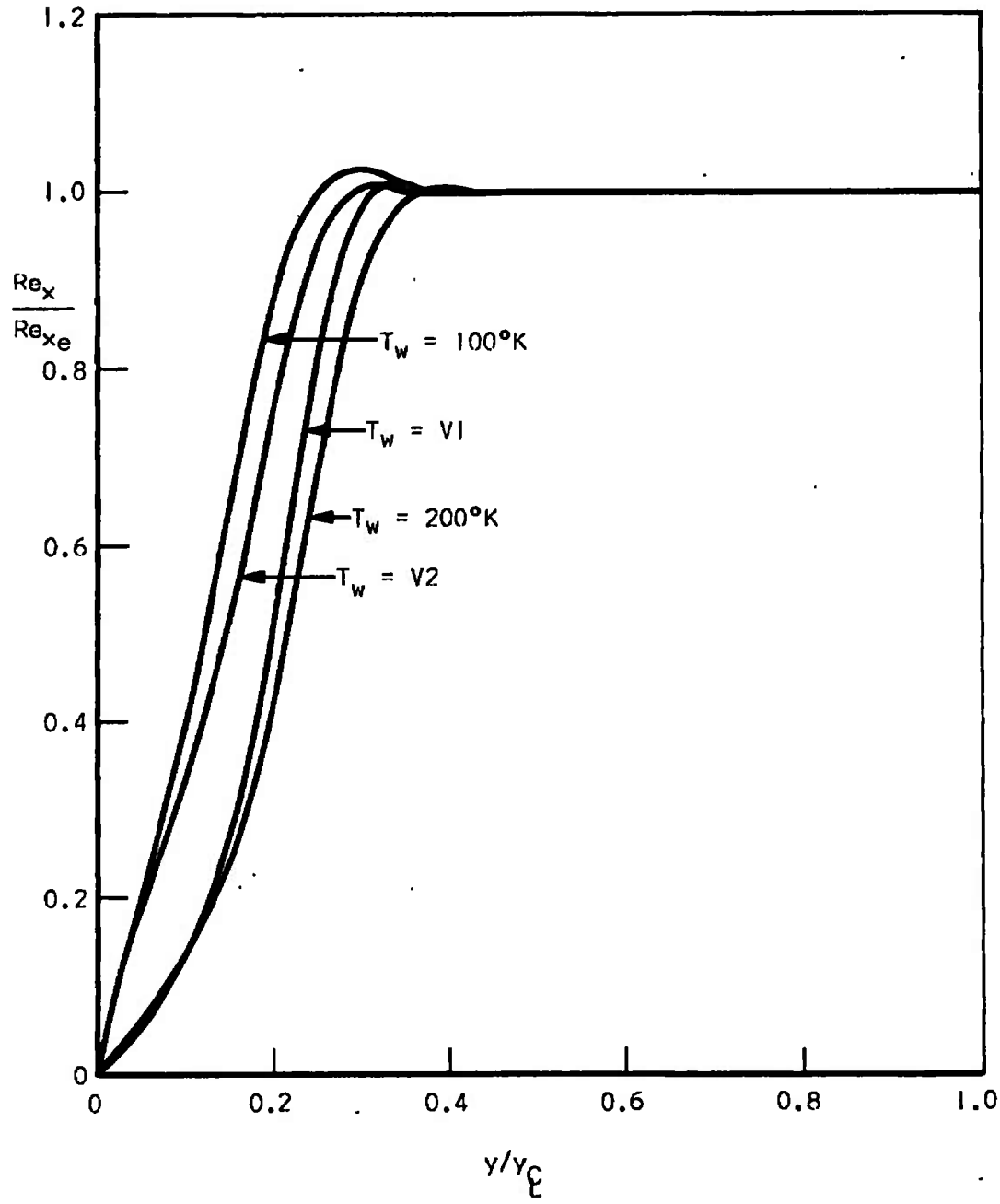

Fig. 9 Plot of Reynolds Number Distributions at Mach Three Nozzle Exit

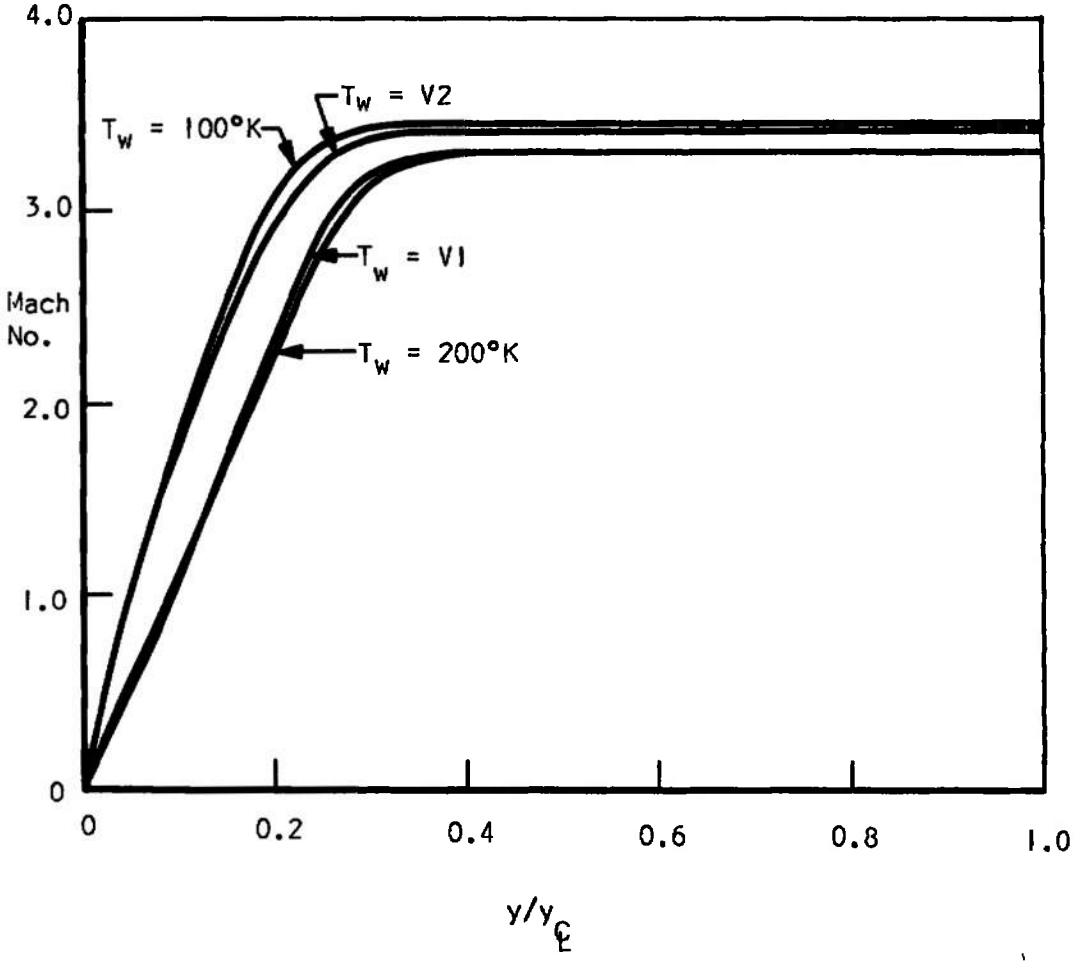

Fig. 10 Plot of Mach Number Distributions at Mach Three Nozzle Exit

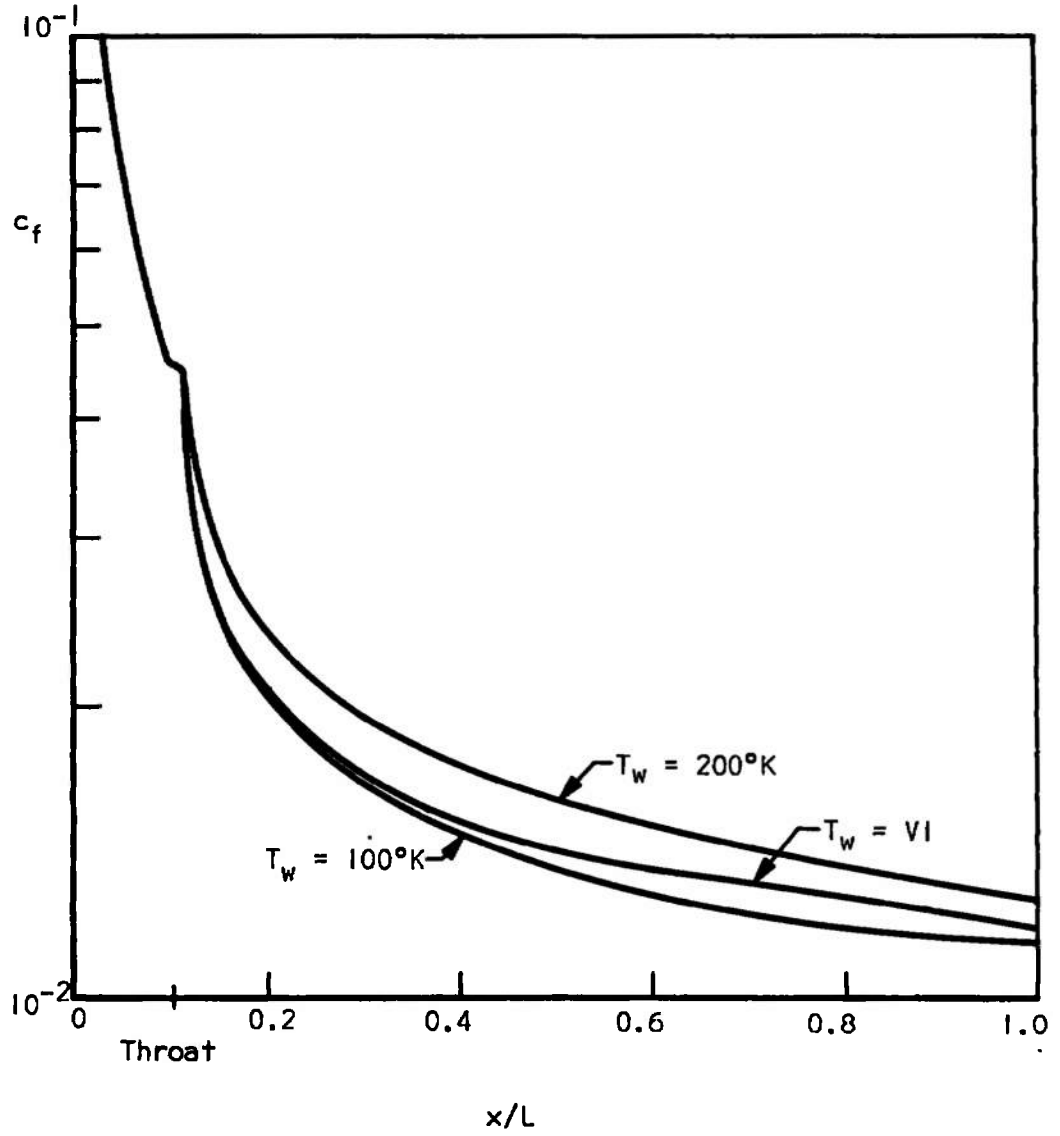

Fig. 11 Skin Friction Coefficients in Mach Three Nozzle

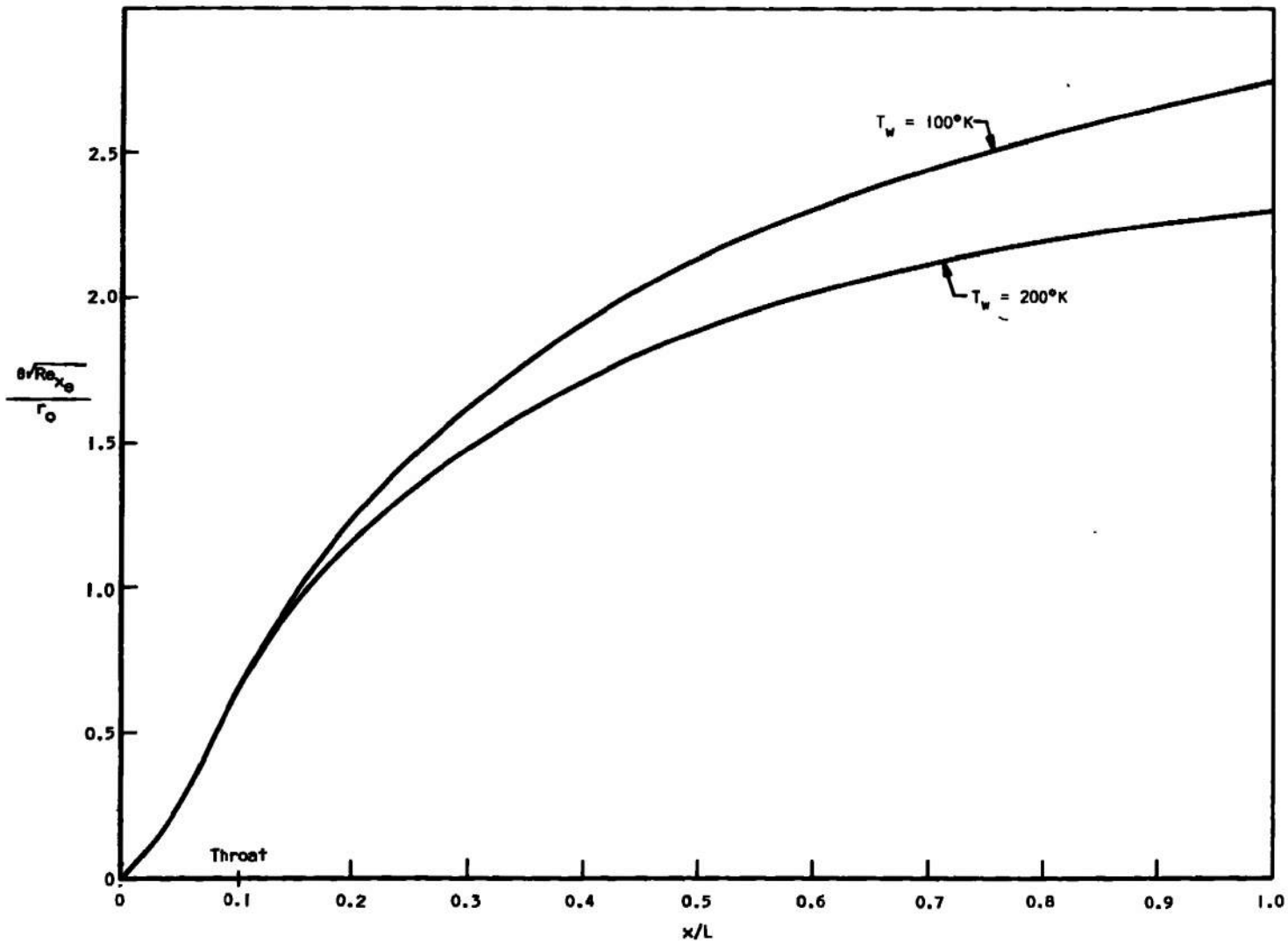

Fig. 12 Normalized Momentum Thickness Distributions in Mach Three Nozzle

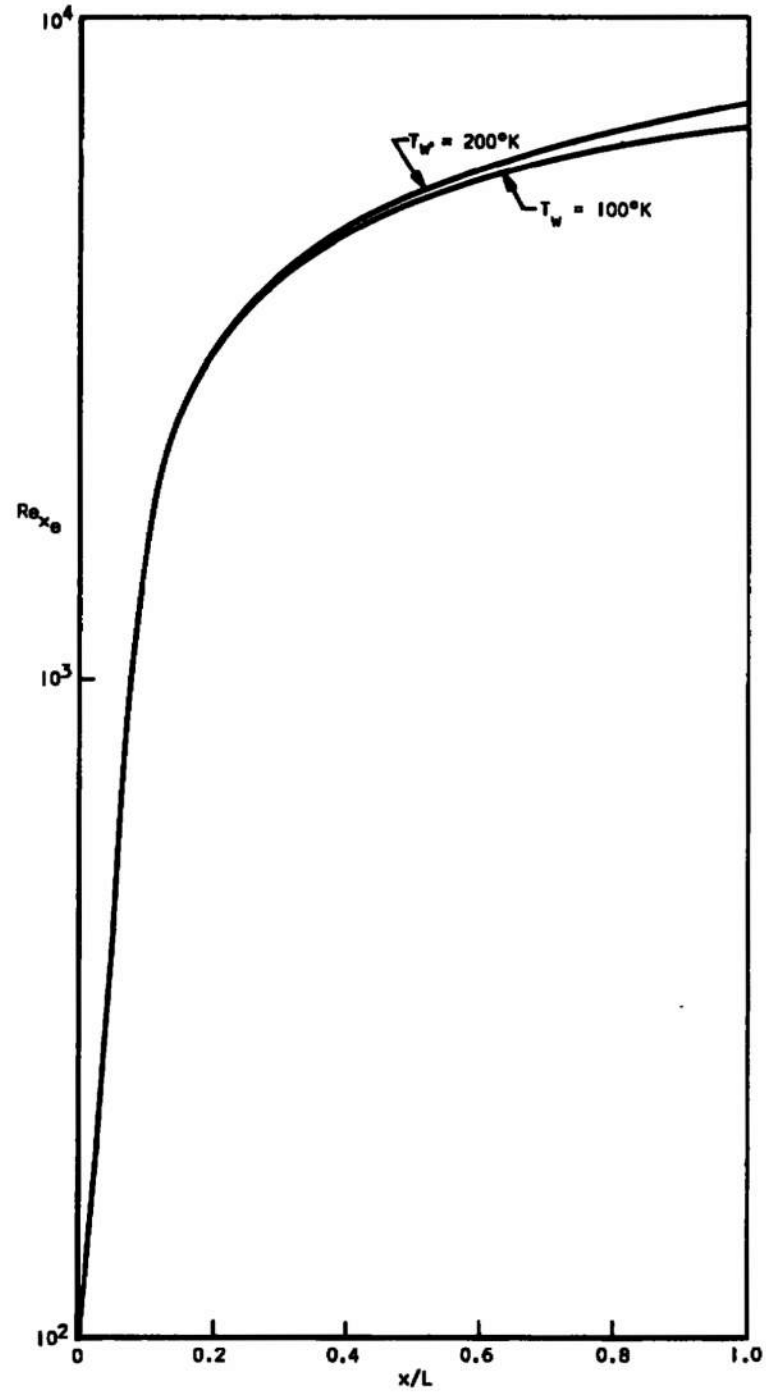

Fig. 13 Plot of Centerline Reynolds Number Distributions in Mach Three Nozzle

The Reynolds number profile given in Figure 9 indicates that a relatively constant Reynolds number region may exist that is larger than the isentropic core region. This is due to the slight "dip" in the static temperature profile near the edge of the boundary layer which compensates for the velocity dropping off. Such a situation may be desirable for testing purposes when the usable inviscid flow region becomes small.

3.2 SOLUTIONS FOR MACH NINE NOZZLE

The Mach nine nozzle is a contoured water cooled nozzle designed by the method of Potter and Durand. It operates in Tunnel L of the von Kármán Facility. This nozzle was designed for a Mach number of 9.0 at plenum chamber conditions of T_o = 2365°K and P_o = 30.0 psia.

From the work of Kinslow and Miller (10), it has been concluded that the vibrational modes freeze somewhere upstream of the throat for this particular nozzle and conditions. Therefore, effective values of T_o and P_o were selected to yield the actual gas properties in the free-stream assuming frozen flow throughout. The values used were T_o = 2475°K and P_o = 30.9 psia.

From the assumption of free-stream frozen flow, one might be concerned about the possibility of vibrational relaxation existing in the portion of the boundary layer near the wall. Such a situation might occur due to lower velocities in this region permitting more molecular collisions per unit length and, thus, relaxational effects may exist. However, it will be shown later that the solution given by assuming vibrationally frozen flow agrees with experiment data.

Therefore, it is concluded that if vibrational relaxation exists across the boundary layer, it is negligible for this particular condition.

Various results from the solution for the Mach nine nozzle with a constant wall temperature of 322°K are presented in Figures 14 through 18. This wall temperature is estimated to be the actual one existing in the nozzle. An approximately constant wall temperature occurs due to the cooling arrangement.

The effect of wall temperature on Stanton number, momentum thickness, displacement thickness, and boundary layer thickness is shown in Figures 19 and 20. These solutions were obtained for the same pressure distribution and two different constant wall temperatures of T_w = 100°K and T_w = 333°K. The displacement thickness is reduced about the same amount as the boundary layer thickness. However, these solutions are not indicative of the actual boundary layer that would exist in the nozzle for these two wall temperatures since the solutions were not iterated.

3.3 SOLUTIONS FOR MACH TEN NOZZLE

The Mach ten nozzle is also a water-cooled contoured nozzle designed by the method of Potter and Durand which operates in Tunnel L of the von Kármán Facility. This nozzle was designed to operate at a Mach number of 10.0 and plenum chamber conditions of T_o = 3090°K and P_o = 18.0 psia.

The work of Reference 10 indicates that the flow in this nozzle is vibrationally frozen downstream of the throat. The effective

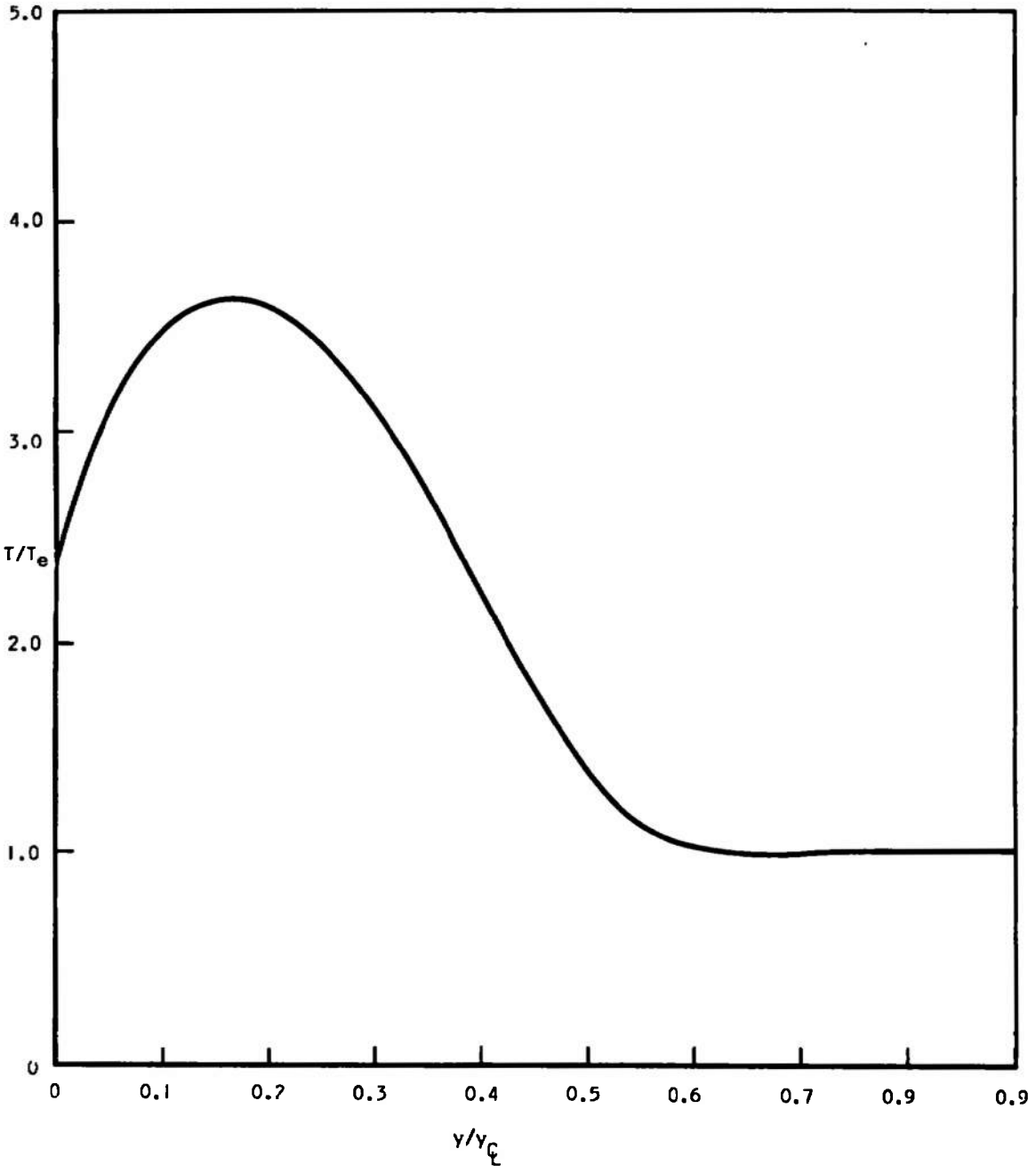

Fig. 14 Static Temperature Distribution at Mach Nine Nozzle Exit, T_e= 136°K

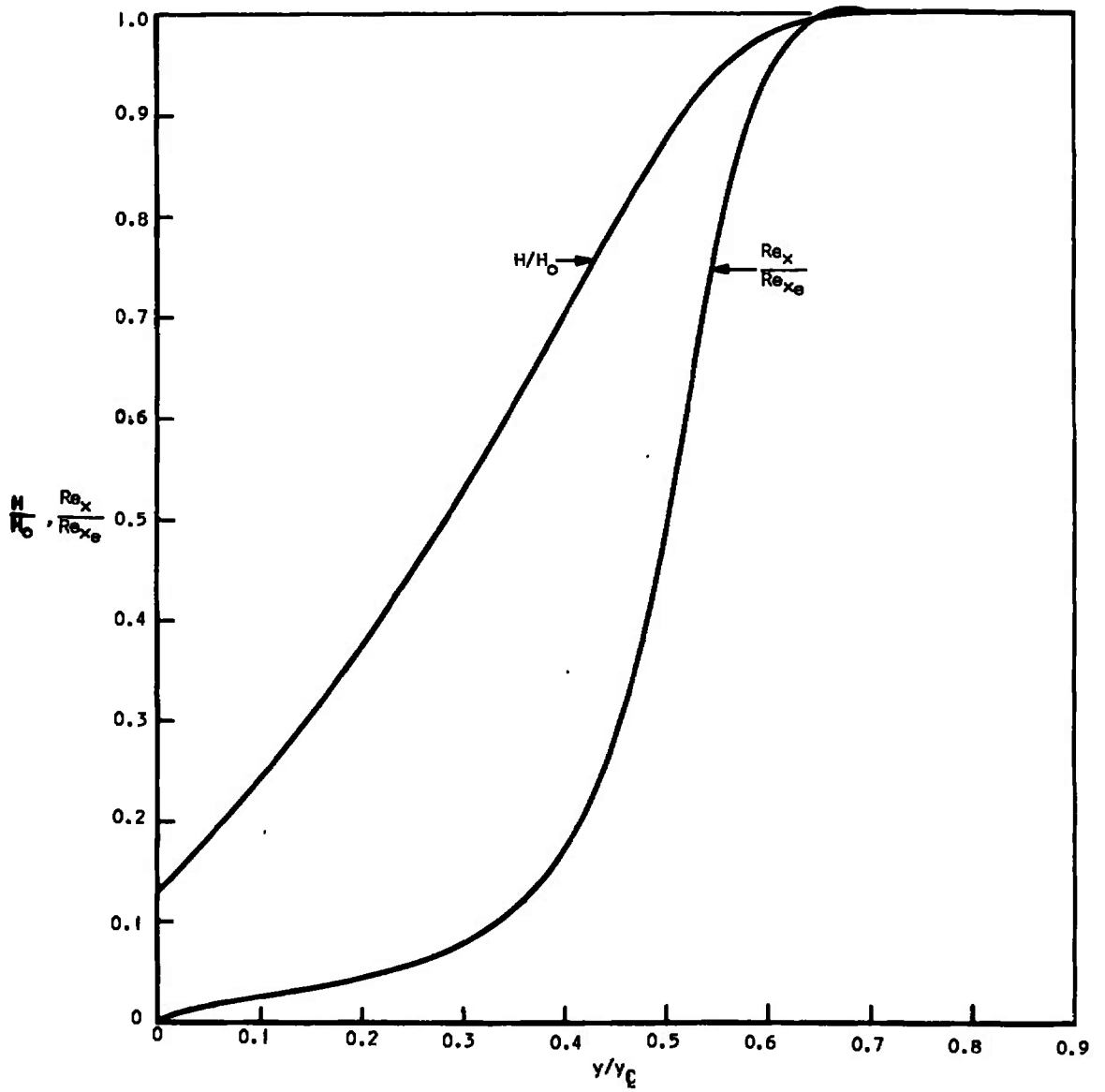

Fig. 15 Total Enthalpy and Reynolds Number Distributions at Mach Nine Nozzle Exit, Re FT^{-1} = 15,000

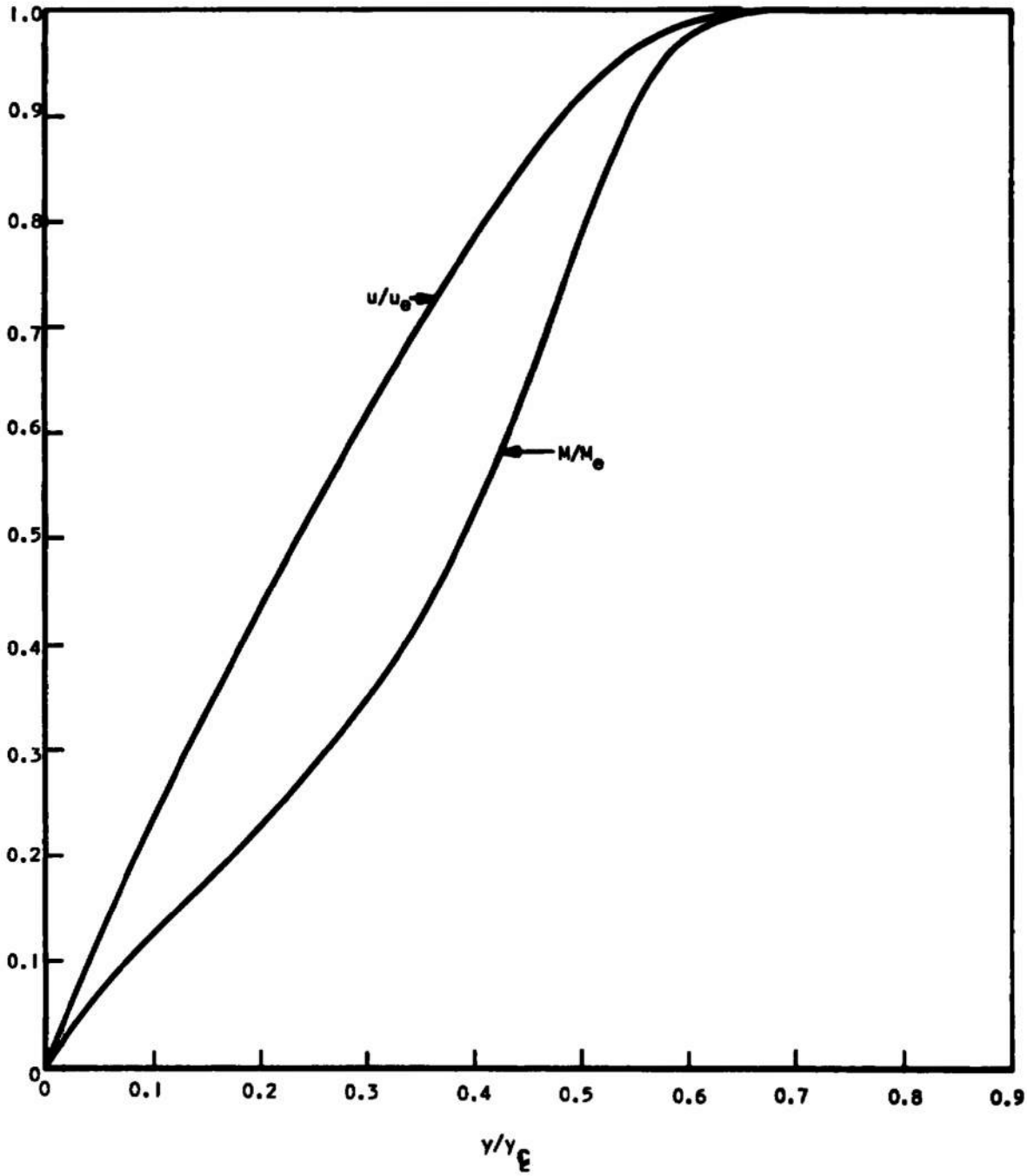

Fig. 16 Mach Number and Velocity Distributions at Mach Nine Nozzle Exit, H_w/H_o = 0.13, M_e = 9.263

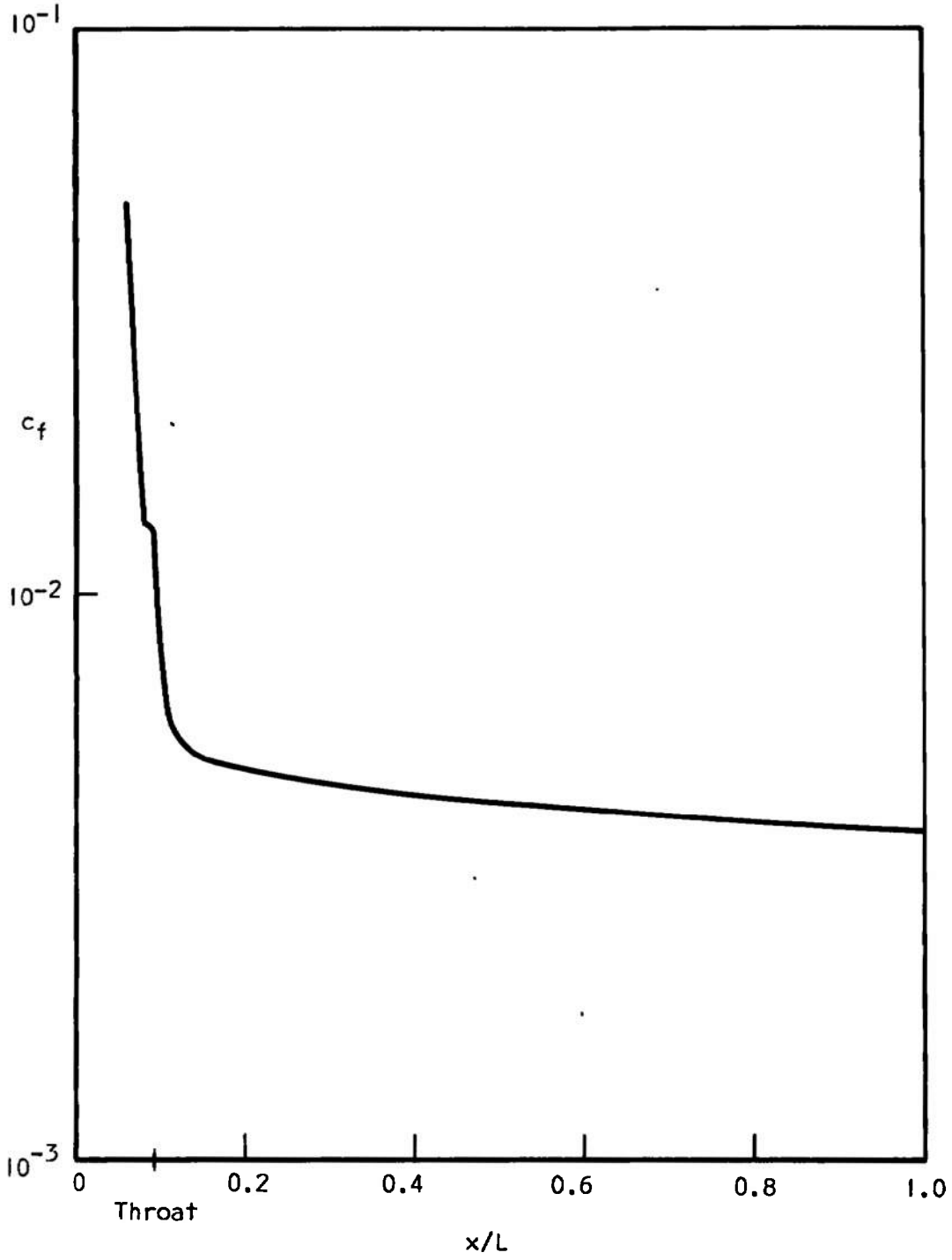

Fig. 17 Skin Friction Coefficient in Mach Nine Nozzle, H_w/H_o = 0.13

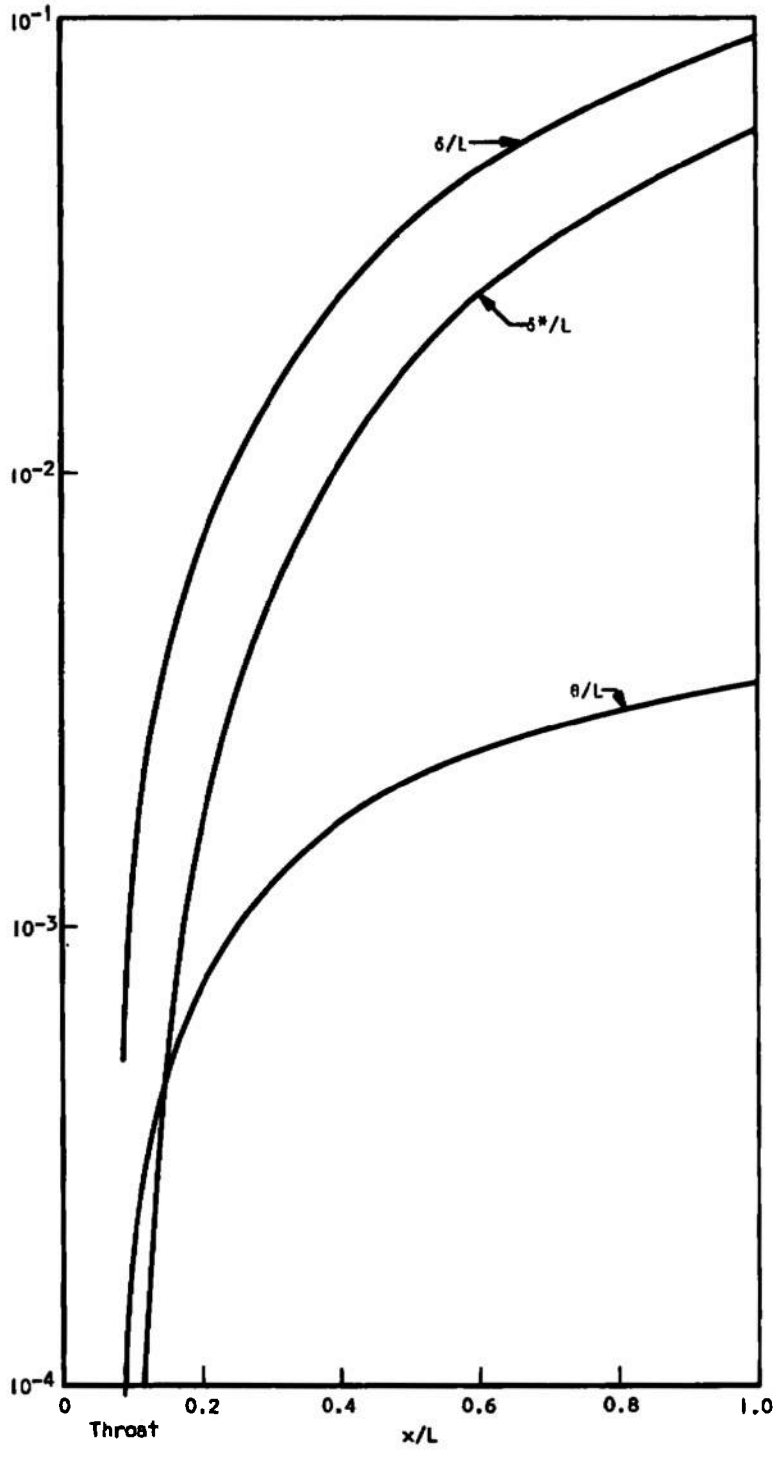

Fig. 18 Momentum, Displacement, and Boundary Layer Thicknesses in Mach Nine Nozzle, H_w/H_o = 0.13

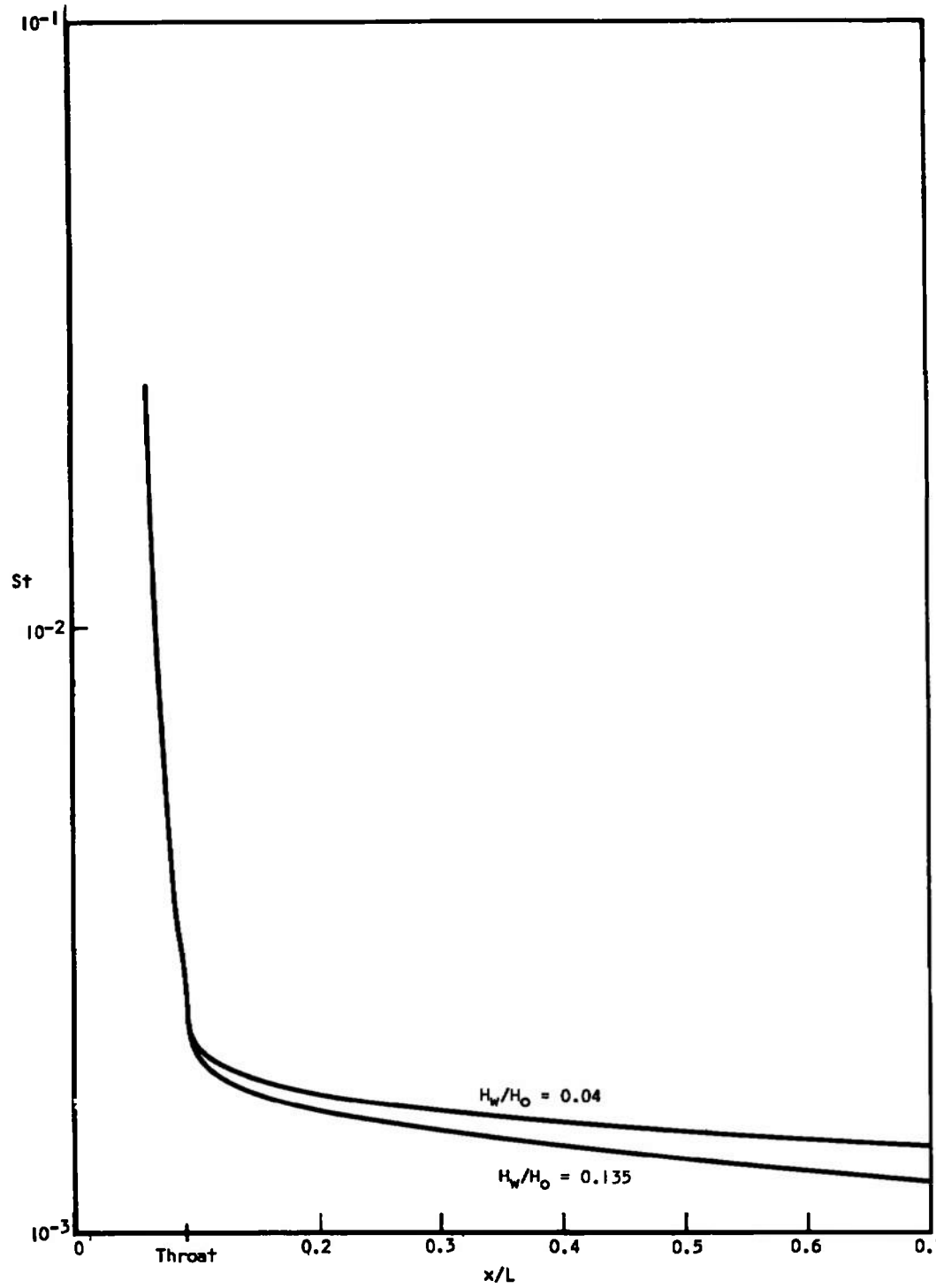

Fig. 19 Plot of Stanton Number in Mach Nine Nozzle for a Prescribed Pressure Distribution

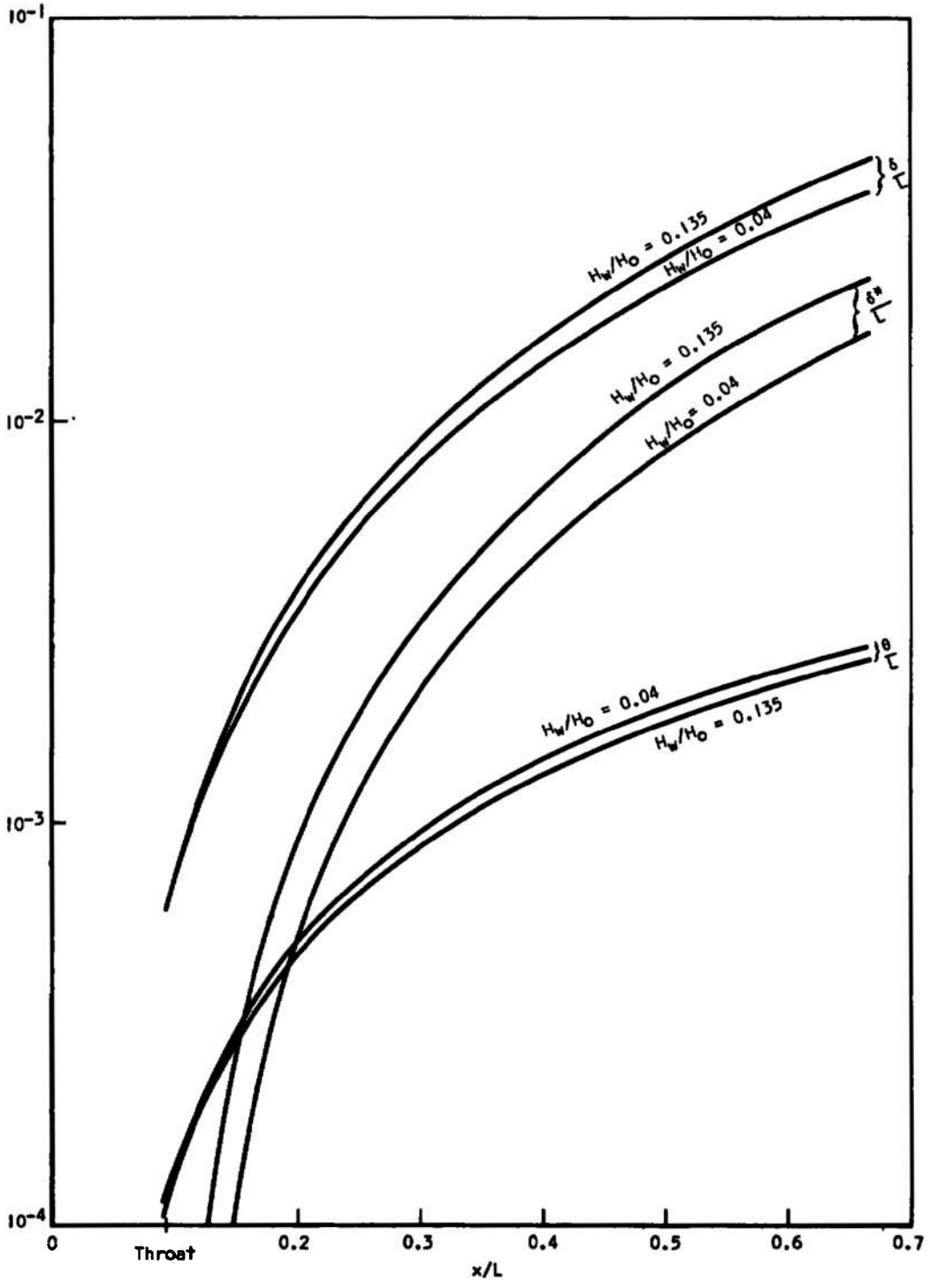

Fig. 20 Plot of Momentum, Displacement, and Boundary Layer Thicknesses in Mach Nine Nozzle for a Prescribed Pressure Distribution

T_o and P_o used with the assumption of frozen flow throughout the nozzle was T_o = 3120°K and P_o = 18.58 psia. The wall temperature was taken as constant at 333°K.

Solutions for this nozzle were calculated to compare with experimental heat transfer measurements made by Carden (11). Since the heat transfer rate varies more rapidly near the throat, a smaller step size than usual was taken for the calculations in this region. Solutions were iterated to about two inches downstream of the throat where the heat transfer rate becomes relatively constant and rather small compared to the throat values. The step size taken in this region ranged from 0.020 inches to 0.100 inches depending upon the anticipated pressure gradient at a particular point. It was then increased by about a factor of two without any significant change in the results.

The boundary layer in this nozzle grows very rapidly, and therefore provides a good example of the development of a low density boundary layer with a very large favorable pressure gradient. Figures 21 through 25 illustrate the development of the boundary layer in the throat region. Figure 22 indicates that the Mach number at the throat is nearly constant through most of the boundary layer due to the nature of the velocity and temperature distributions. Notice in Figure 25 that negative displacement thicknesses were obtained through the converging region to about 0.25 inches downstream of the throat. The distributions in Figure 26 are the results of the initial input pressure distribution since successive iterations were not obtained in this region. However, it should be indicative of the type of distributions which would exist

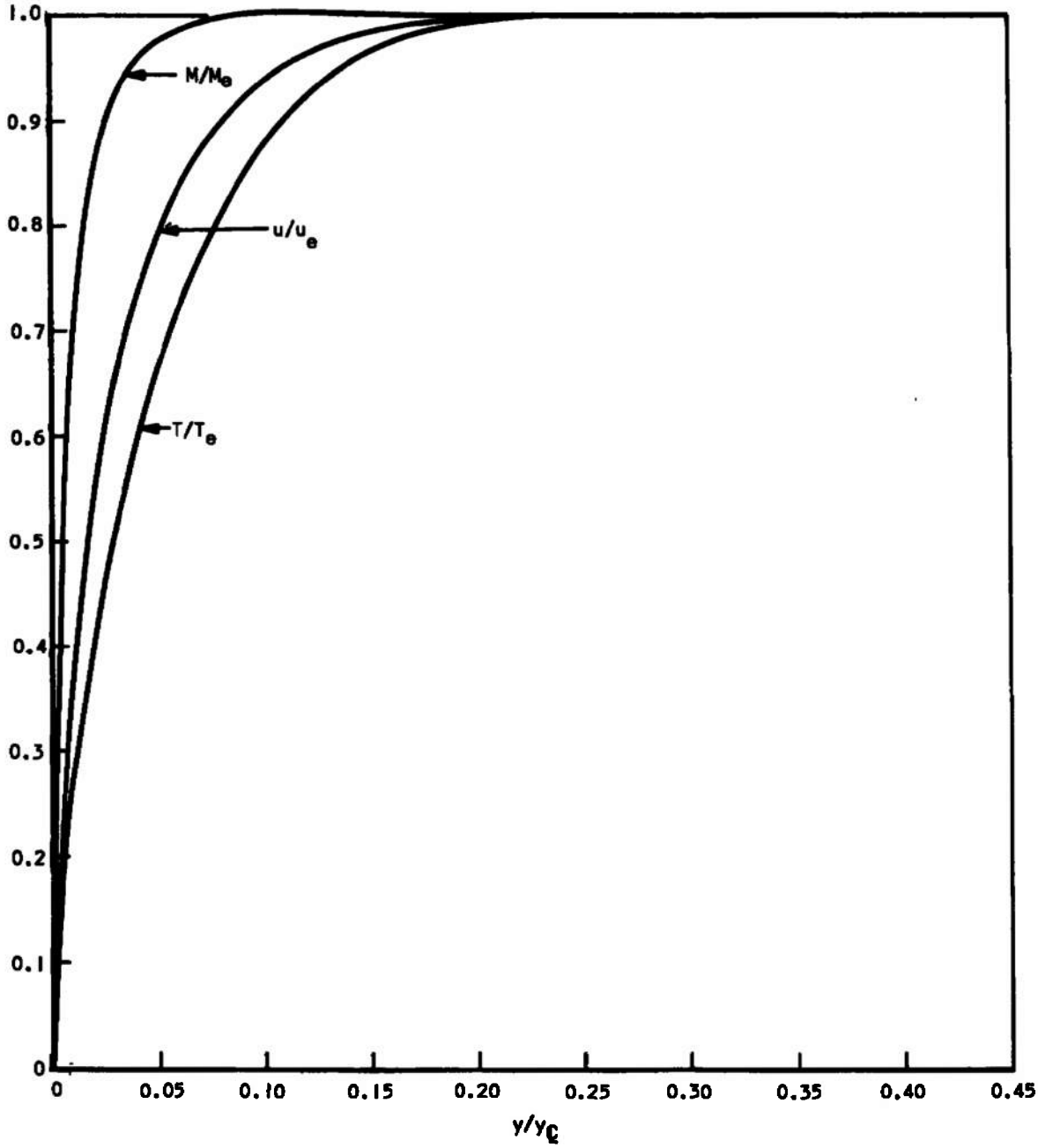

Fig. 21 Velocity, Mach Number, and Static Temperature Distributions at 0.16 Inches Upstream of Mach Ten Nozzle Throat, M_e = 0.459

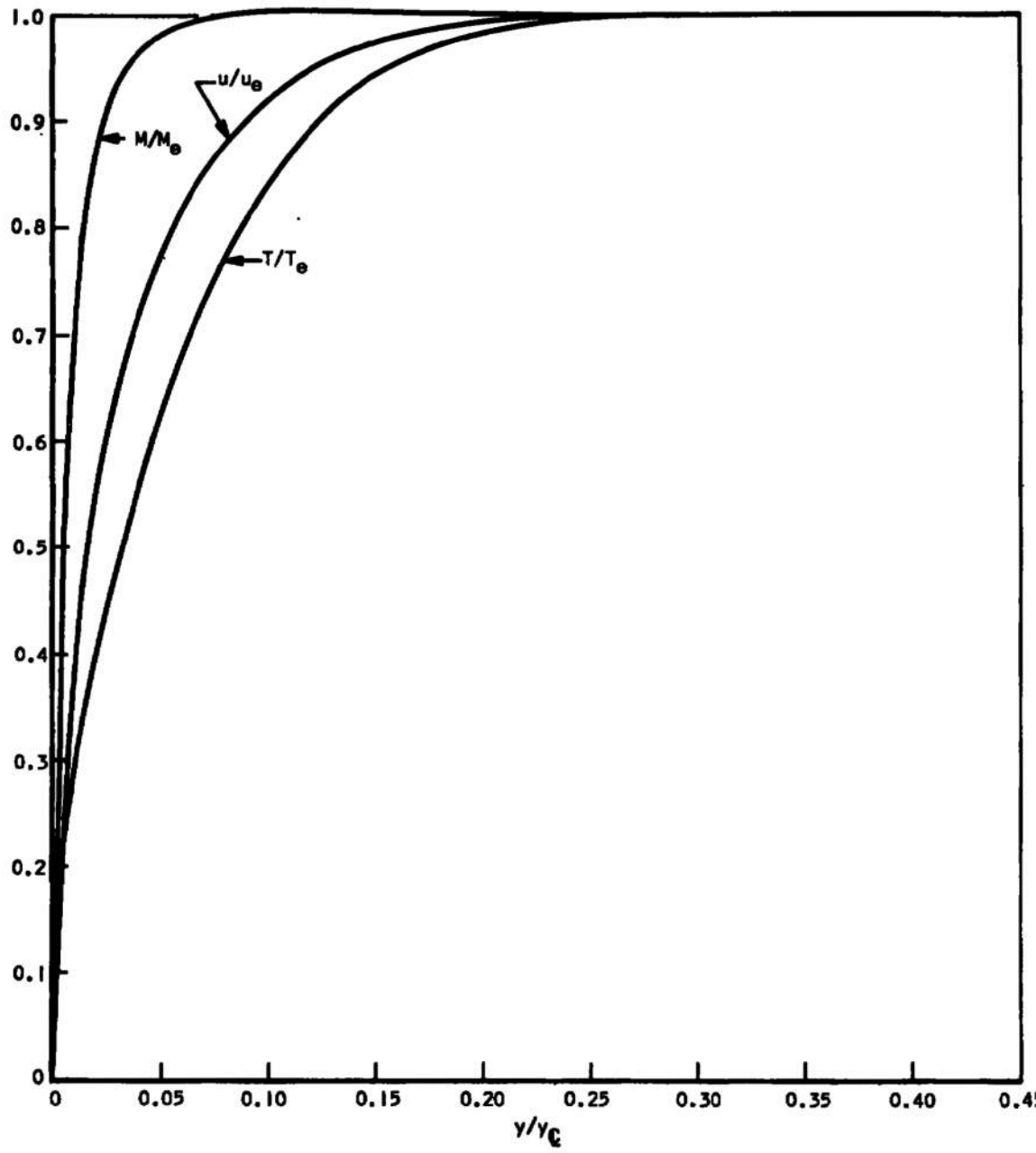

Fig. 22 Velocity, Mach Number, and Static Temperature Distributions at Mach Ten Nozzle Throat

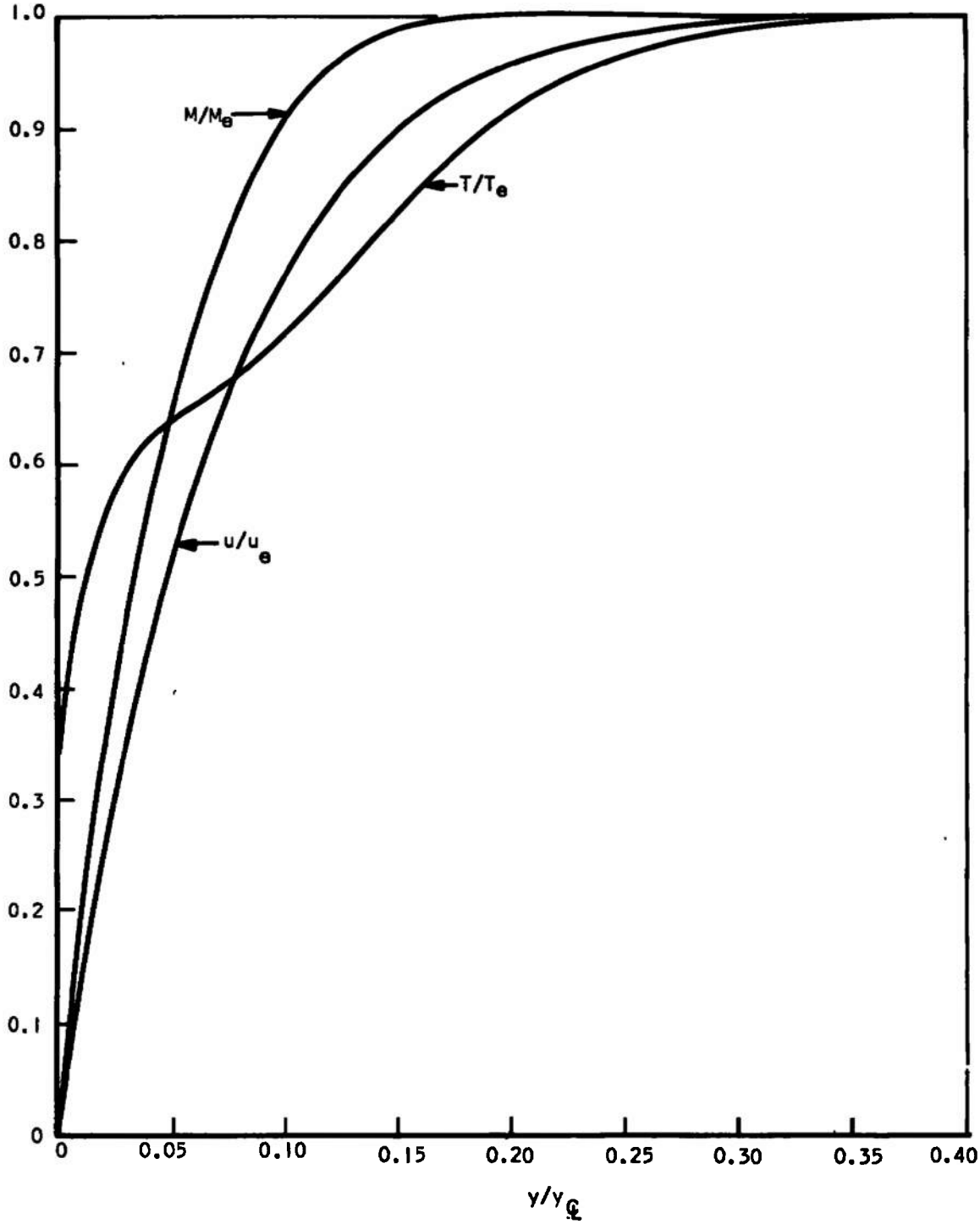

Fig. 23. Velocity, Mach Number, and Static Temperature Distributions at 0.51 Inches Downstream of Mach Ten Nozzle Throat, M_e = 3.331

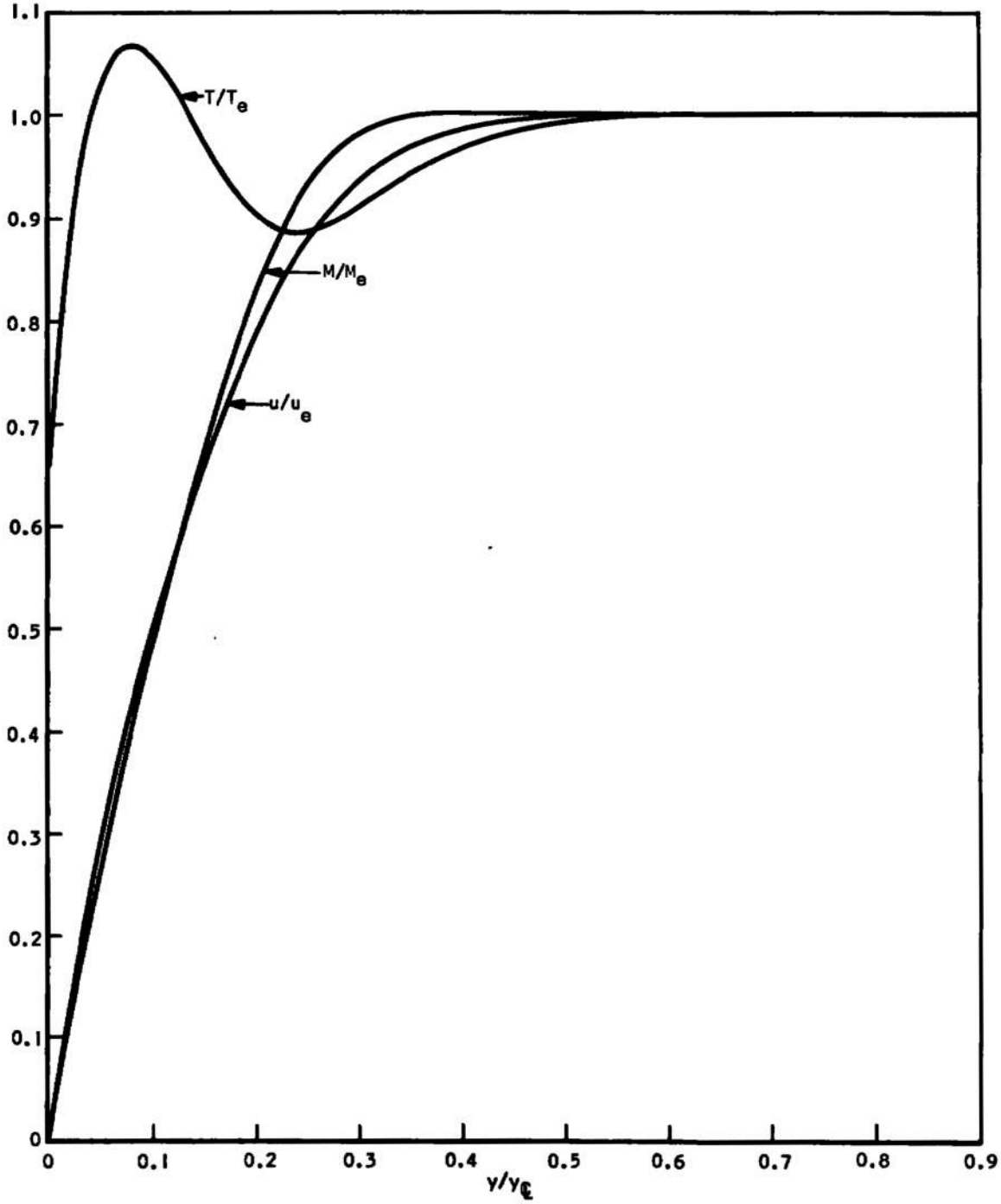

Fig. 24 Velocity, Mach Number, and Static Temperature Distributions at 1.57 Inches Downstream of Mach Ten Nozzle Throat, M_e = 5.094

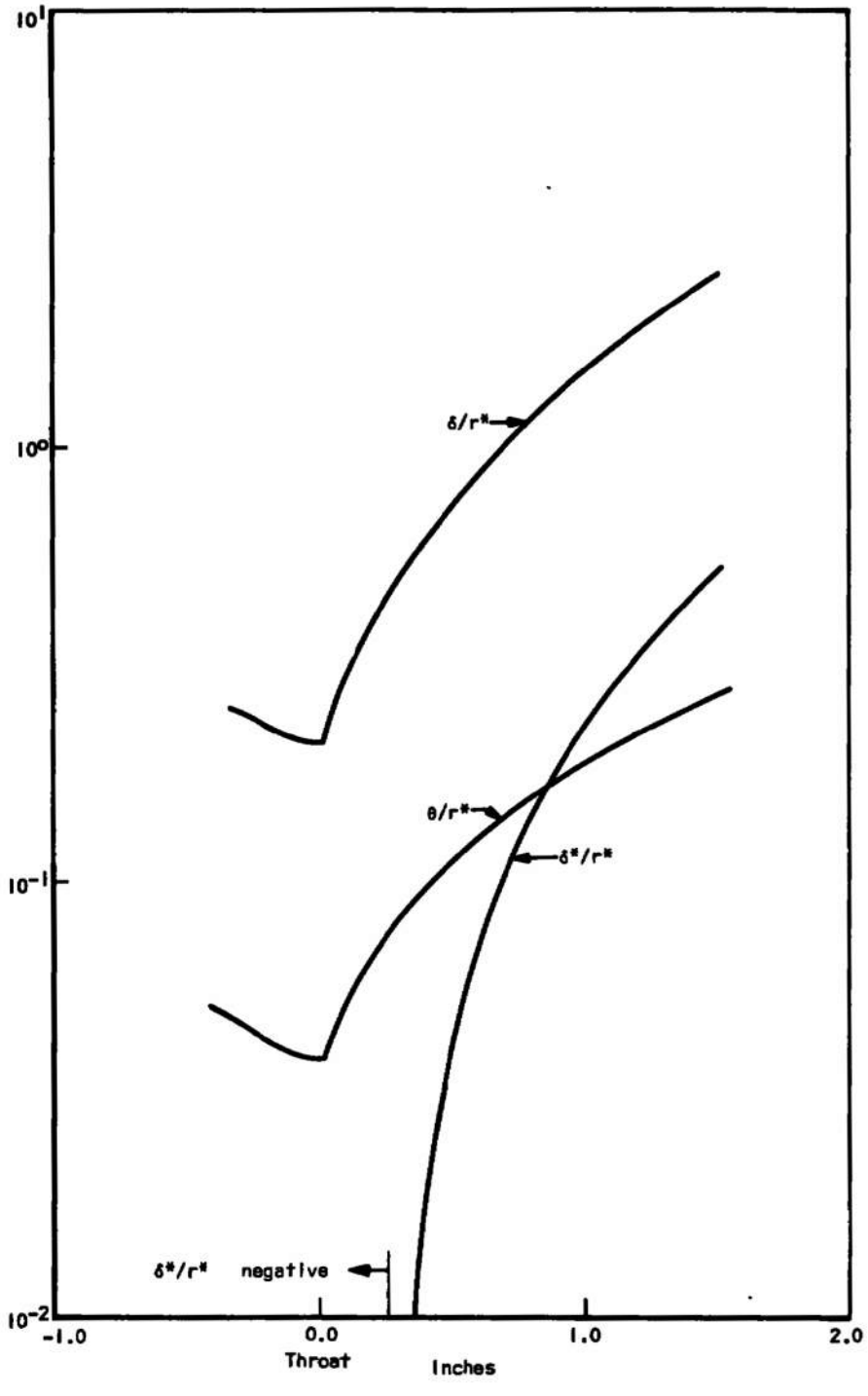

Fig. 25 Momentum, Displacement, and Boundary Layer Thicknesses in Throat Region of Mach Ten Nozzle

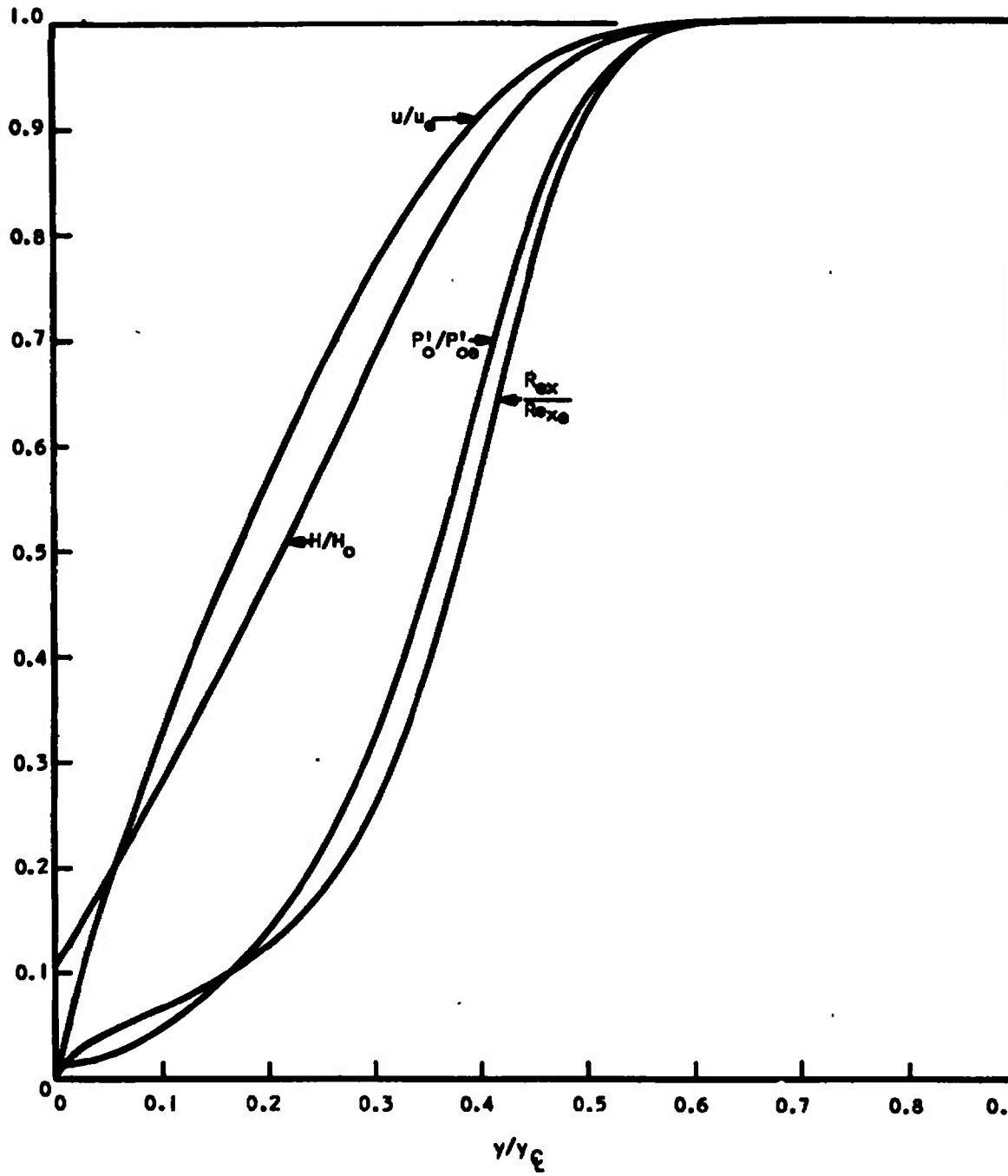

Fig. 26 Plot of Indicated Distributions at 10.20 Inches Downstream of Mach Ten Nozzle Throat

across the boundary layer farther downstream.

The plane at 1.57 inches downstream of the throat is located at only 14 per cent of the total axial distance of the nozzle, but a Mach number of 5.094 has been reached which is about half of the exit value of 10.15. The velocity at this point has attained 93 per cent of the exit value. Such an expansion, and associated pressure gradient, provides an excellent test for the theoretical solutions.

3.4 SOLUTIONS FOR MACH EIGHTEEN NOZZLE

The Mach eighteen nozzle is a water-cooled 14° half-angle conical nozzle which operates in Tunnel M of the von Kármán Facility. The plenum chamber conditions used for this nozzle were T_o = 6160°K and P_o = 203 psia, and the wall temperature was taken as constant at 300°K.

Solutions for this nozzle were iterated twice in an attempt to "bracket" the final result. One might suspect that such a thing can be done by referring to Figure 2, page 23. In Figure 2 the initial input pressure distribution was more favorable than actually existed in the nozzle, and the first two iterations bracketed the final result. By initially inputting a less favorable pressure distribution than was expected to exist in the nozzle, it is anticipated that the first two iterations would again bracket the final result. The reason for such an oscillation is that a less favorable pressure gradient would produce a thinner boundary layer and then the new pressure gradient calculated would be larger than the first and hence the next iteration would yield a thick boundary layer. This oscillation seems to occur in each case;

however, as has already been pointed out, the convergence is very rapid after two or three iterations.

The second iteration was not carried out completely as indicated in Figures 27 and 28 by the dashed lines. The reason was that the machine time required for this second iteration was too long. The initial input pressure distribution consists of many closely spaced values permitting a smooth distribution and hence good streamwise derivatives. With a smooth distribution of properties along the centerline a relatively large step size could be taken for the first iteration. However, this caused numerical problems in the second iteration since the new pressure distribution could only be calculated from the few stations used in the first iteration. The streamwise derivatives were then not as accurate due to the few points available for calculating the derivatives. Rather than use more stations in the second iteration or curve fit the calculated pressures in order to smooth the streamwise derivatives, the second iteration was extrapolated in Figures 27 and 28 by the nature of the first iteration. Some results of these iterations are given in Figures 27, 28, and 29.

3.5 COMPARISON OF SOME OF THE SOLUTIONS

As shown in Figure 4, page 25, for the Mach three nozzle, the effect of wall cooling is to produce a larger relative reduction in displacement thickness than in boundary layer thickness. This produces a somewhat surprising result in that a nozzle designed for a certain Mach number and throat size will have a smaller area of uniform core if the

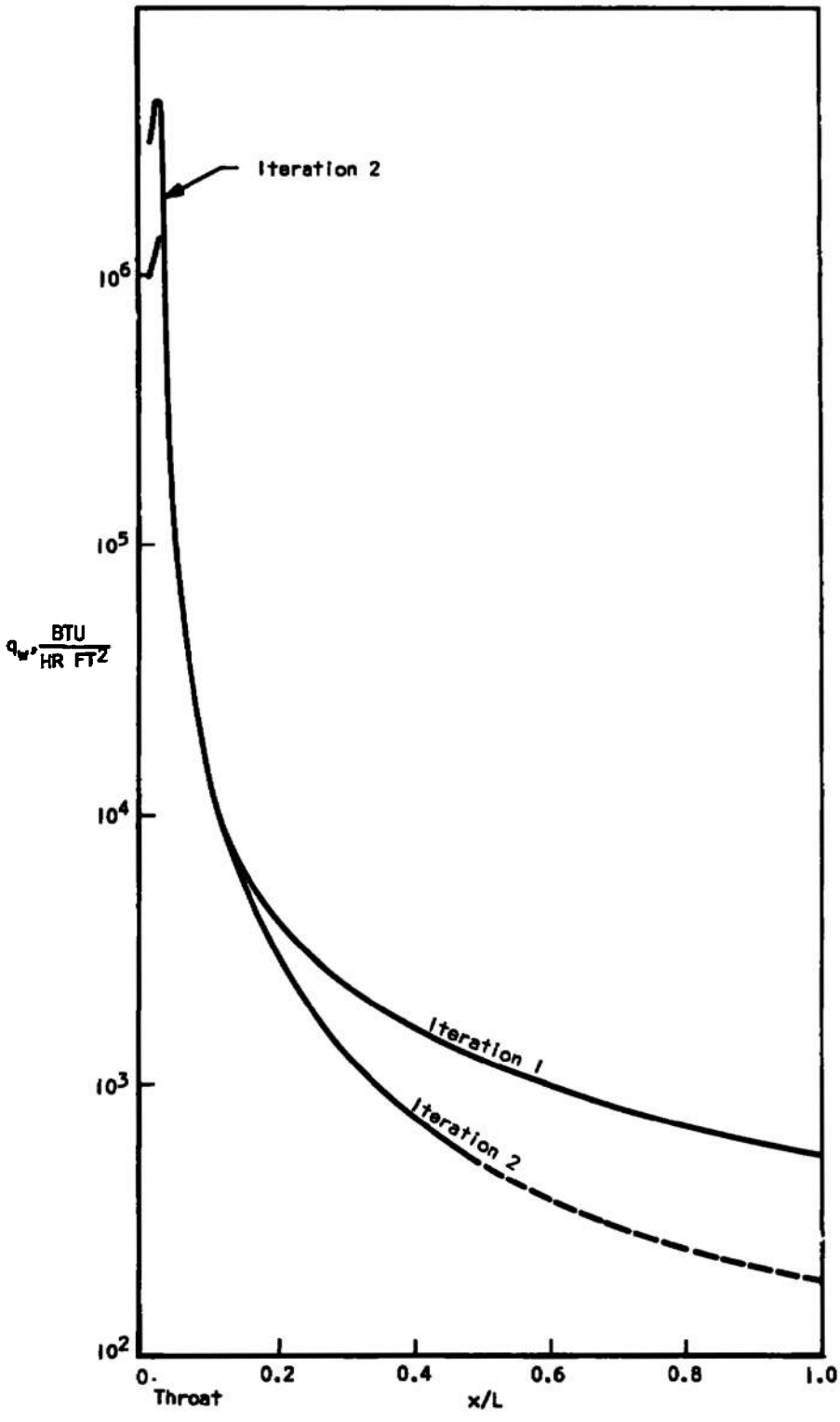

Fig. 27 Heat Transfer Rate in Mach Eighteen Nozzle

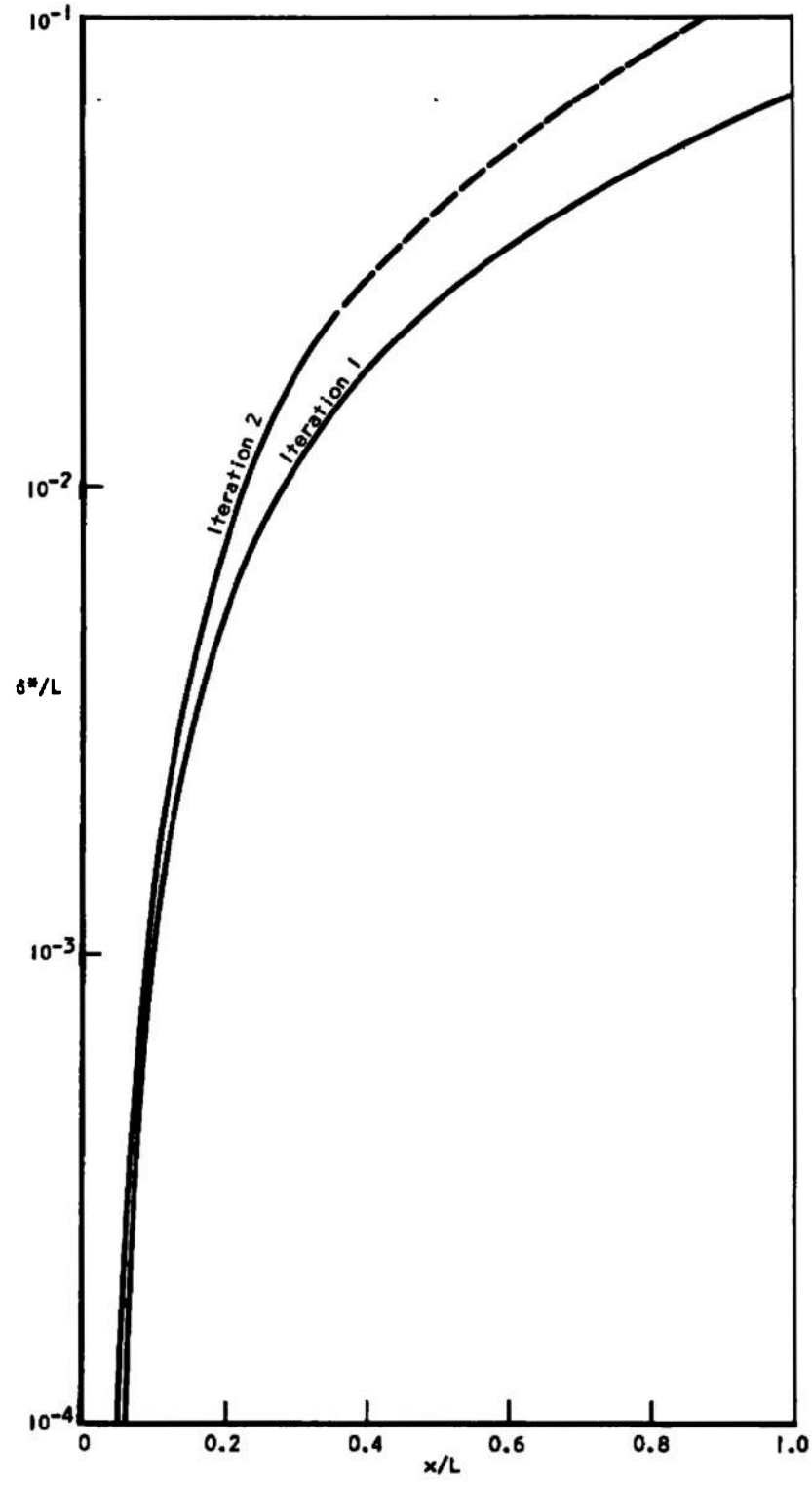

Fig. 28 Displacement Thickness in Mach Eighteen Nozzle

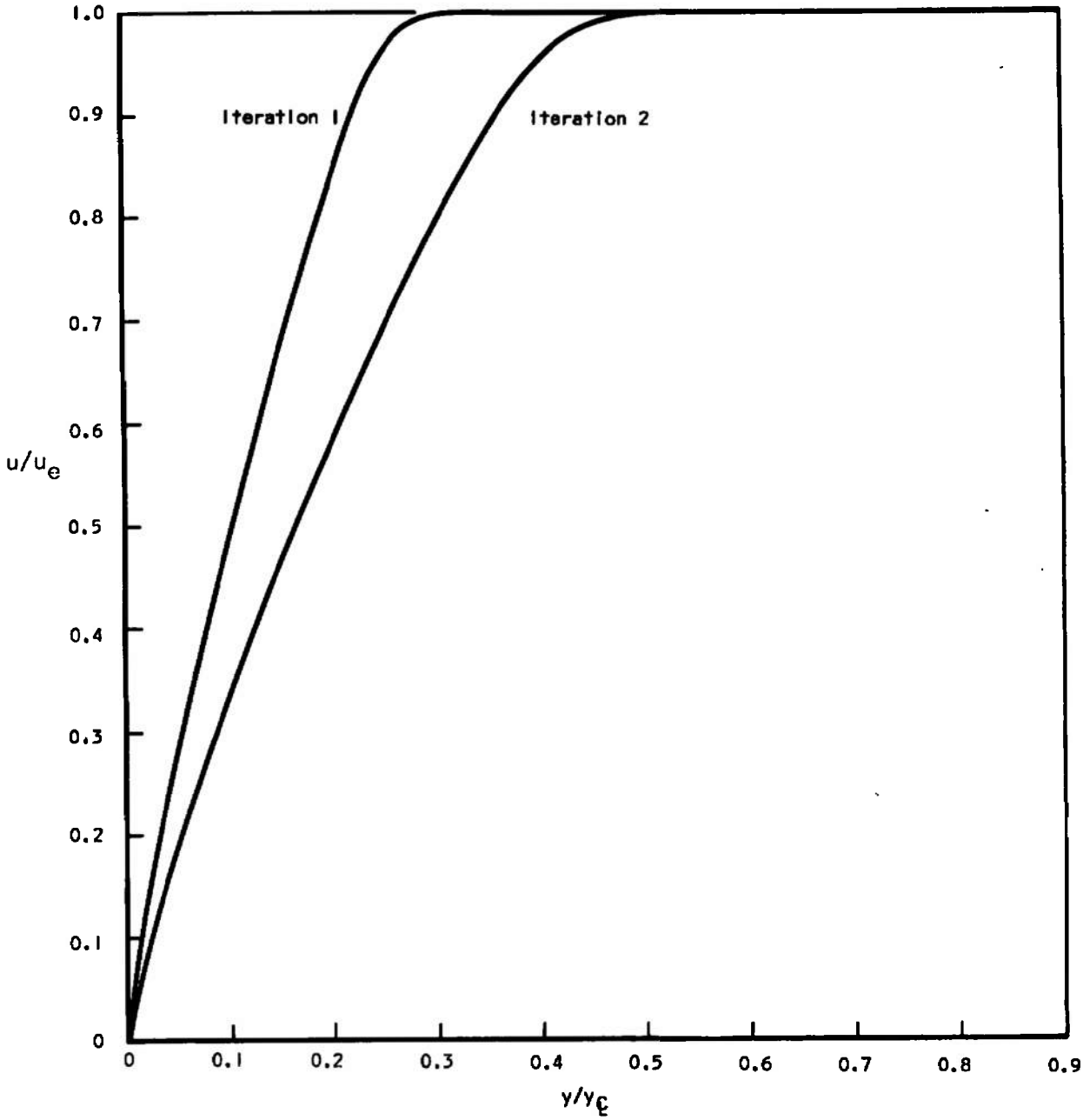

Fig. 29 Velocity Distributions from First and Second Iterations of Mach Eighteen Nozzle Solution at 19.42 Inches Downstream of Throat

nozzle is designed for a cold wall rather than a hot wall. The reason for this is that the nozzle wall must be changed for each design rather than the effective inviscid radius, and therefore, the size of the uniform core is less for the cold wall since the difference between the displacement and boundary layer thickness is greater. Of course, the actual nozzle radius for the hotter wall will be larger, and hence the wall angle will be greater since the throat in each case is the same size. Therefore, the limitation of designing nozzles with hot walls is governed by the permissible physical size of the nozzle and the maximum expansion angle the flow can stand without separating. Potter and Carden give an example of the design of a given Mach number nozzle which clearly illustrates a reduction in uniform core due to using a cold wall.

However, if one is interested in increasing the size of the uniform flow of a given nozzle, extreme wall cooling is an advantage. As pointed out earlier, a significant axial gradient may also occur which might be alleviated somewhat by a variable wall temperature.

It is necessary in using integral techniques to assume an appropriate velocity profile. Some of the more simple analytical expressions used for the velocity are given and plotted in Figure 30. The exponent ζ has been altered slightly in the expression

$$\frac{u}{u_e} = \sin\left(\frac{\pi}{2}\zeta\right) \tag{54}$$

in an attempt to get better agreement and still keep the expression simple. The boundary layer thickness used here is that defined as the point where $u/u_e = 0.995$. In Figure 31, better agreement with the

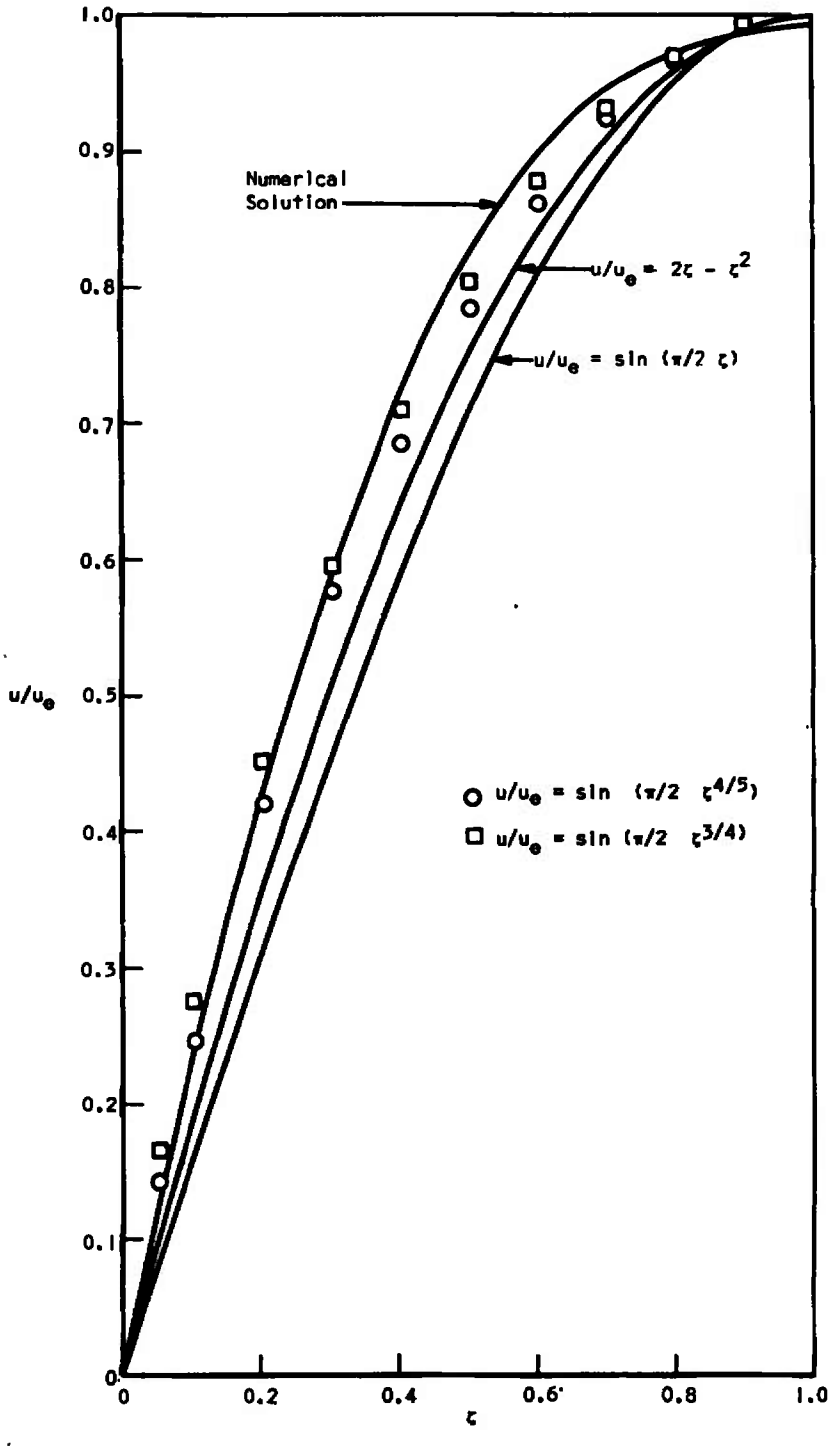

Fig. 30 Plot of Calculated Velocity Distribution at Exit of Mach Three Nozzle for T_w = 100°K, and Some Simple Analytical Expressions

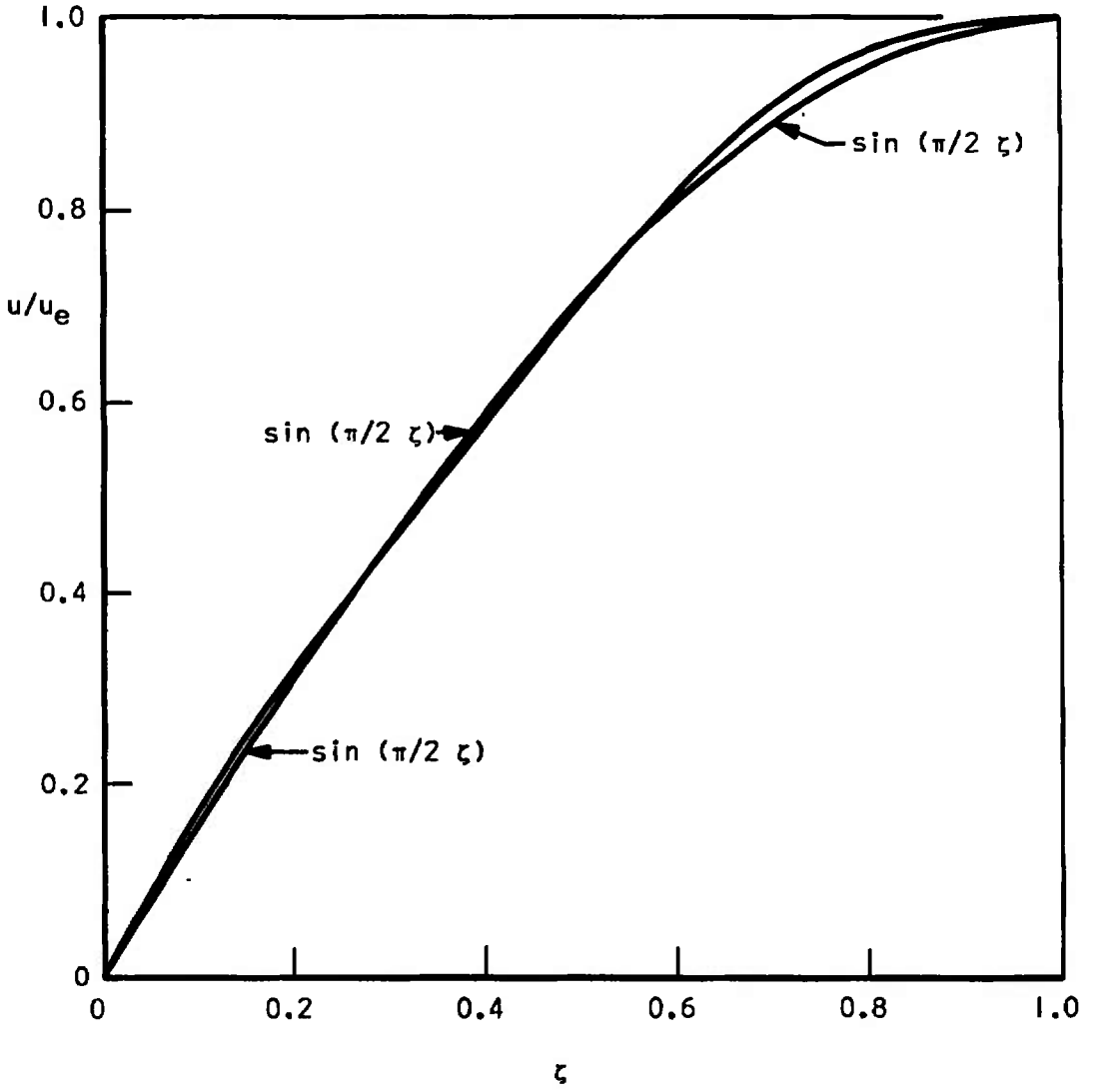

Fig. 31 Plot of Calculated Velocity Distribution at Exit of Mach Nine Nozzle and the Expression $u/u_e = \sin(\pi/2\,\zeta)$

expression given by Equation 54 was obtained by defining the boundary layer thickness as the point where $u/u_e = 0.999$. Since the velocity u approaches u_e asymptotically, there can be a significant difference between the results of the two definitions of boundary layer thickness. It should be noted that if δ is defined by $u/u_e = 0.999$ for the Mach three nozzle case given in Figure 30, the resulting agreement with the indicated expressions is worse. The velocity profiles in the Mach three nozzle all appear to have a near linear portion near the wall, whereas all other profiles appear to have slightly more curve to them near the wall.

The streamwise distributions of $(f'')_w$, $(g')_w$, and β are given in Figures 32 through 34. The x/L value corresponding to a particular point in the nozzle, such as the throat, depends on the particular nozzle considered. However, the relatively sharp "peak" of each curve in Figures 32 through 34 occurs at the throat of the indicated nozzle.

Numerical difficulties were sometimes encountered relatively far downstream near the edge of the boundary layer when the boundary layer approached the thickness of the nozzle radius. This is believed to be due to the transformation variables used. Consider Equation 15 which is the transformation applied to the independent variable y. At a given x location, everything in this equation is constant except ρ, r, and y. Moreover, everything in this equation except ρ, r, and y, is relatively constant for all x values near the exit of the nozzle since u_e and ξ change very little in this region. However, ρ continues to decrease, and therefore, a larger upper limit of integration, y, is

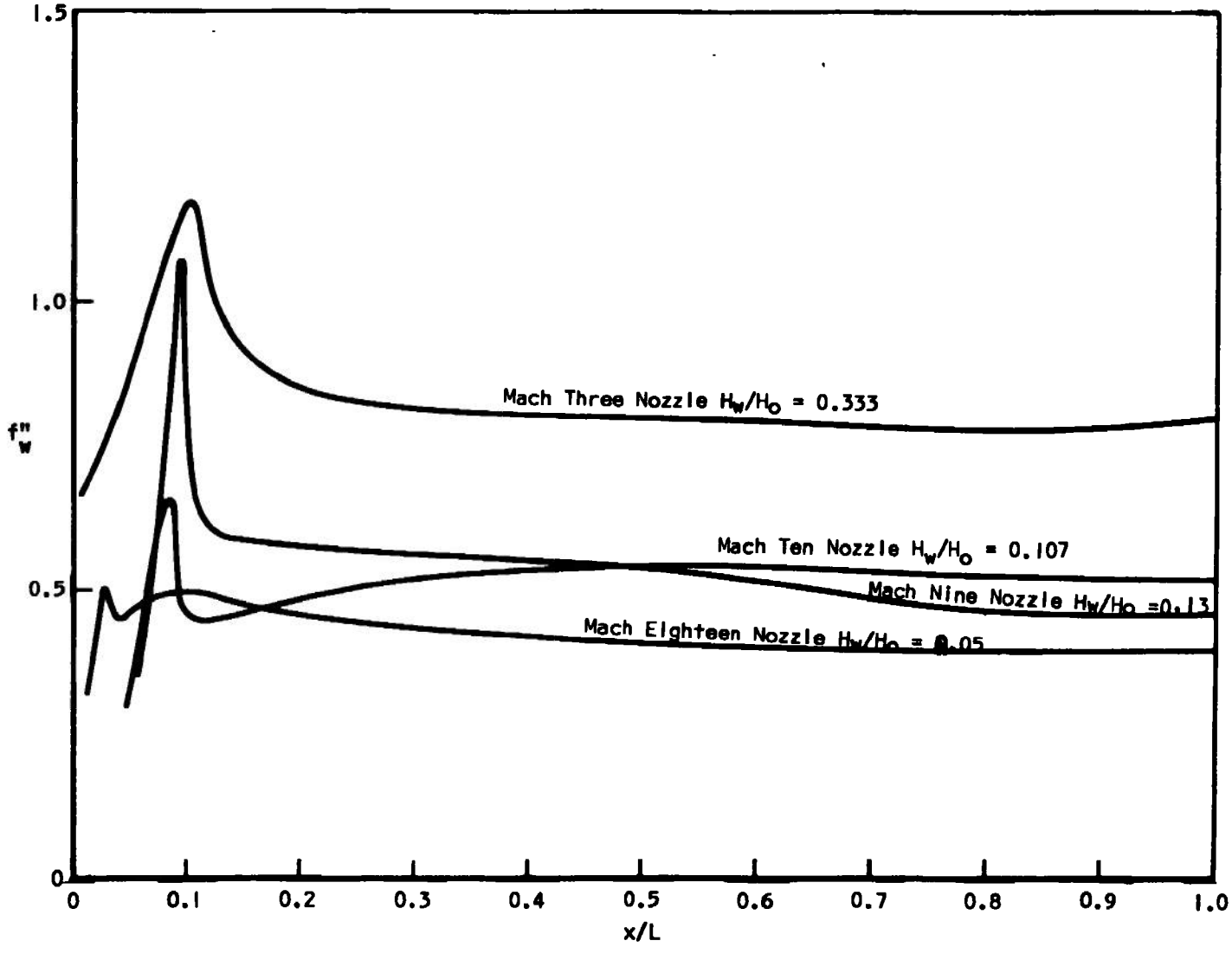

Fig. 32 Distribution of f''_w in Each of the Four Nozzles Considered

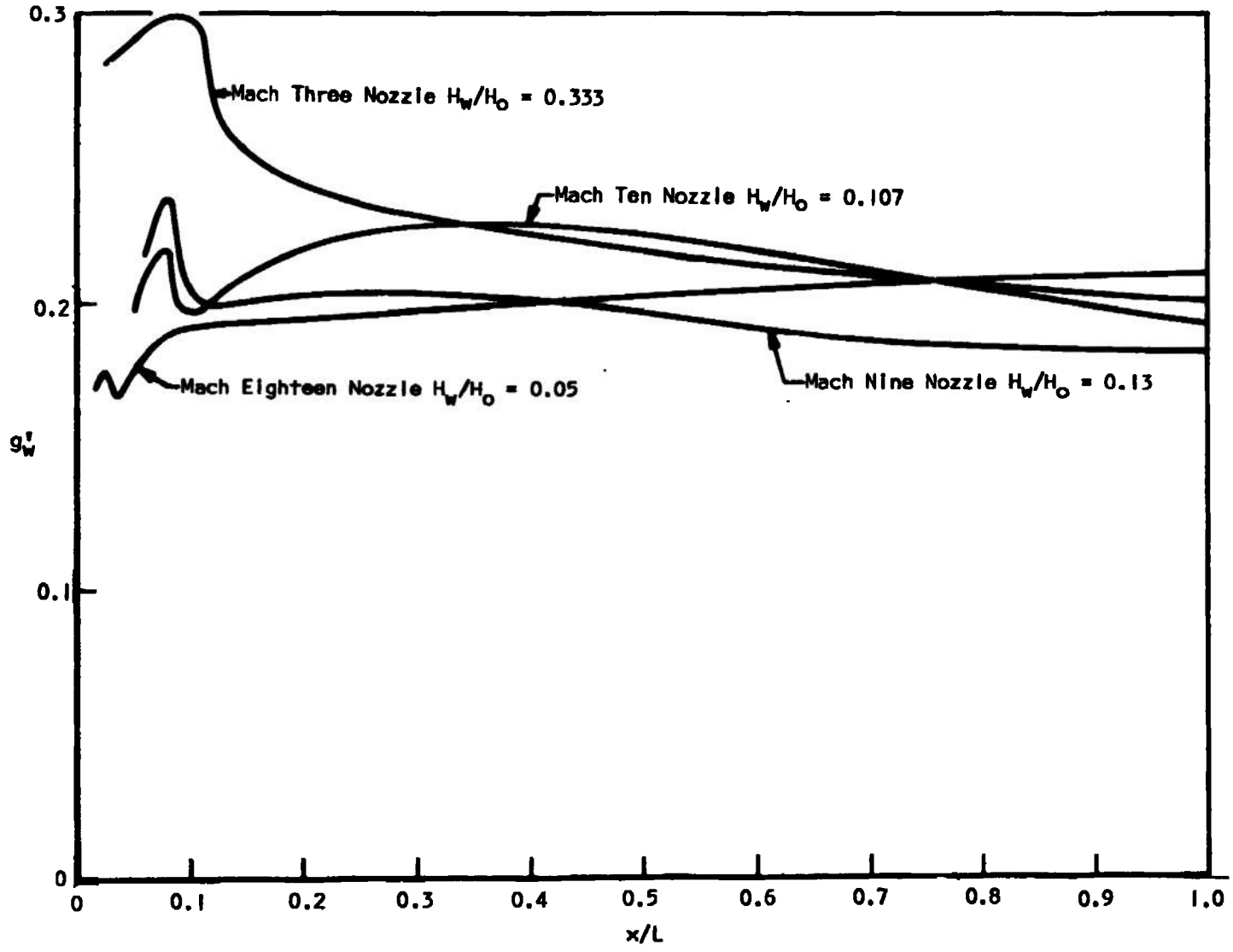

Fig. 33 Distribution of g'_w in Each of the Four Nozzles Considered

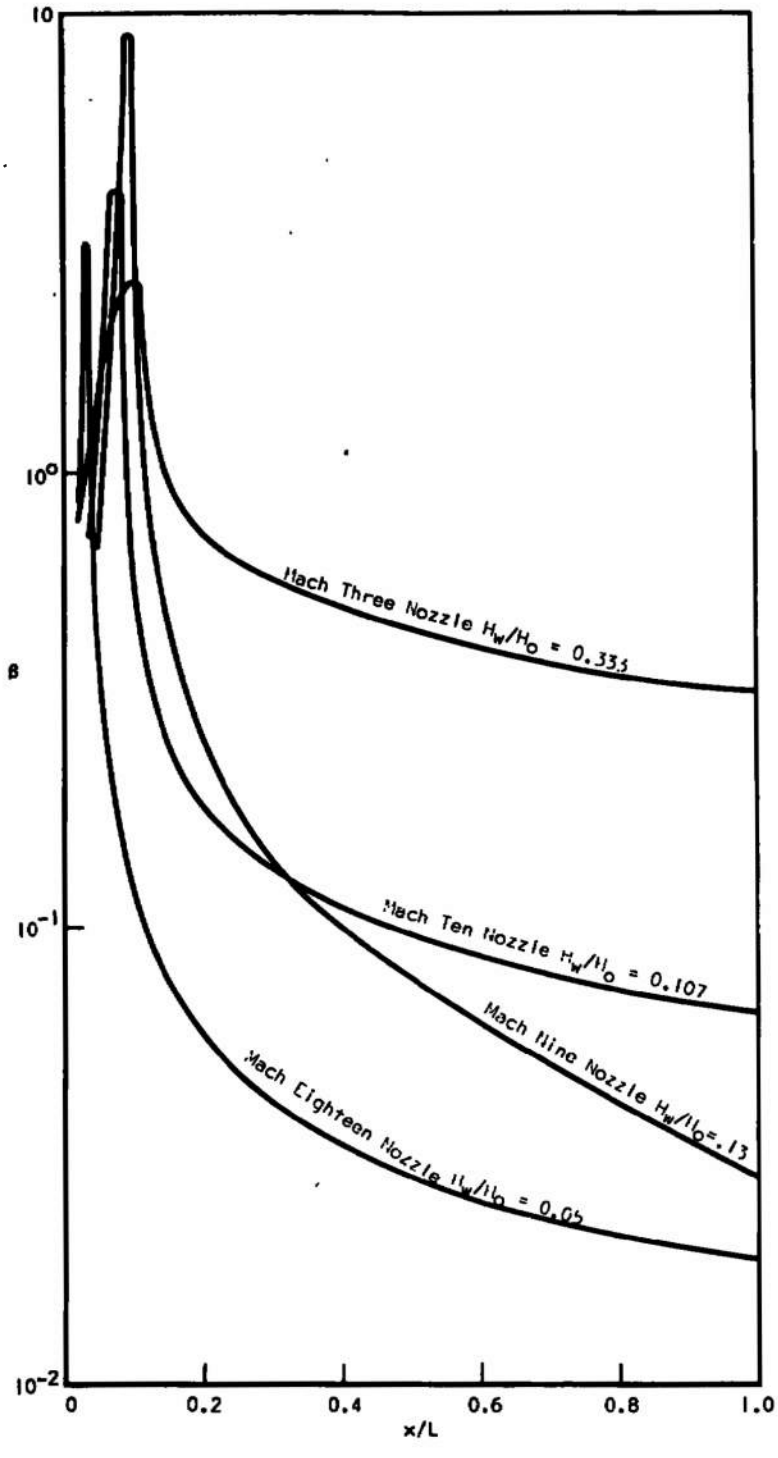

Fig. 34 Distribution of β in Each of the Four Nozzles Considered

required in Equation 15 to satisfy a prescribed value of η. Approximating Equation 15 by writing it in finite difference form, one can see that a given increment of η, which is what the program uses in the numerical integration across the boundary layer, requires an increasing increment in y as the centerline is approached. This increasing increment in y is due to the fact that the variable r is small near the centerline. This increment of y is sometimes too large and convergence is difficult to obtain. Hence, the centerline introduces a problem which does not exist in external boundary layer analysis using the same transformation variables.

SECTION IV
COMPARISON OF THEORETICAL RESULTS AND EXPERIMENTAL DATA

It is not possible to compare the solution of all the dependent variables with corresponding data since appropriate experimental data cannot be obtained. However, the pitot pressure can be obtained experimentally and it provides a somewhat satisfactory test of the theory since it is dependent upon both the velocity and temperature. Carden has made some nozzle wall heat transfer measurements which can be applied to the throat region of the Mach ten nozzle. Also, Potter and Carden present both pitot pressure measurements and relative heat flux measurements taken from the Mach nine nozzle.

The experimental data which are compared to theory consist of measurements of pitot pressure at the exit of the Mach three nozzle, measurements of pitot pressure and relative heat flux for the last three inches of the Mach nine nozzle, and measurements of heat transfer rates of the throat region of the Mach ten nozzle.

Comparison of the measured pitot pressures with the calculated pitot pressure distribution is given in Figure 35 for the Mach three nozzle. The error band represents the accuracy in which the actual location of the pitot pressure probe was known. The reason for the inaccuracy is that the probe was mounted on a remotely controlled moveable support whose position was only known within ±0.5 inches.

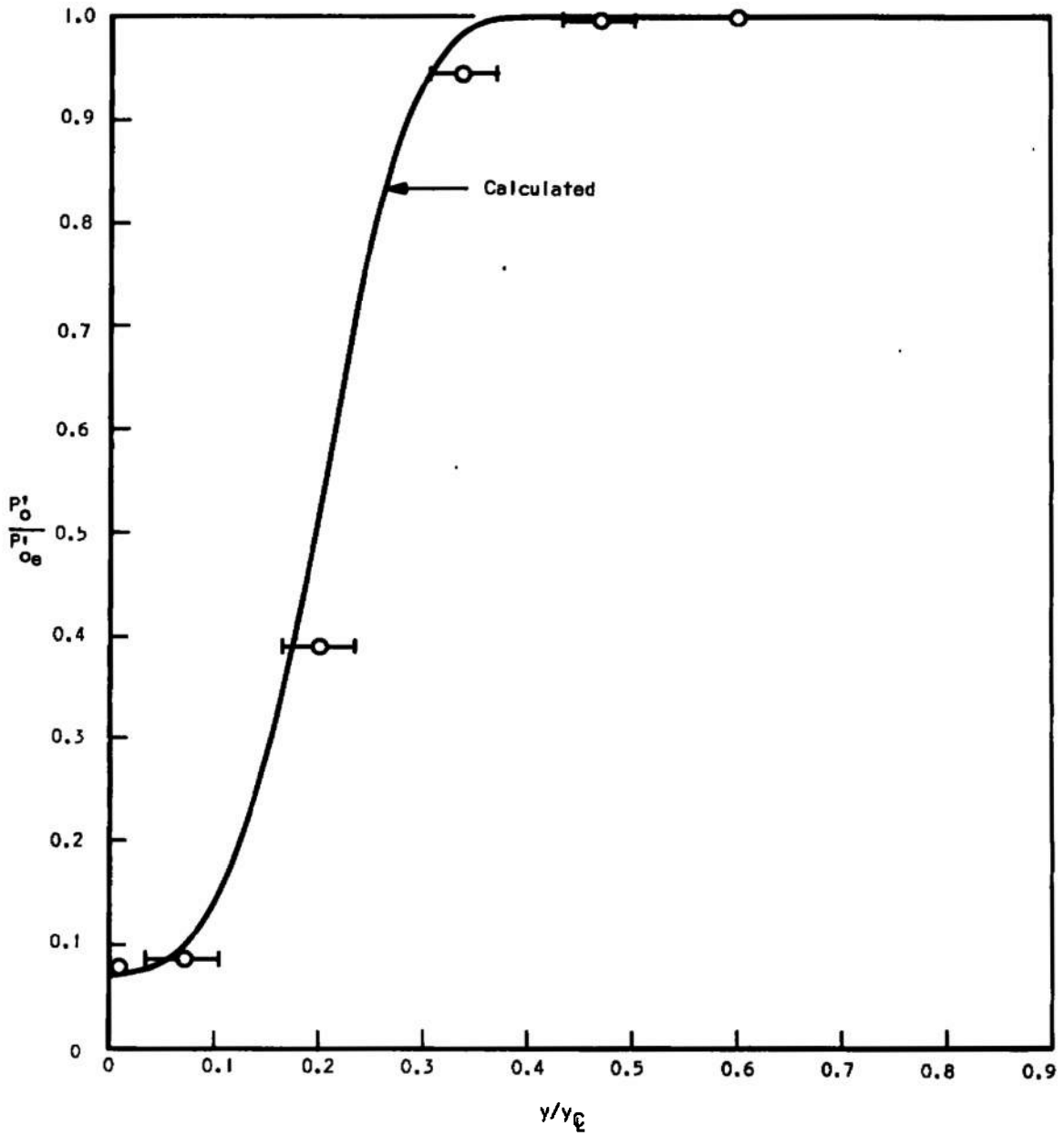

Fig. 35 Plot of Calculated and Measured Pitot Pressure Distributions at Exit of Mach Three Nozzle for T_w = VI

These pitot pressure measurements were corrected for viscous effects by using the calculated Mach number and Reynolds number corresponding to the point of the measurement. The correction required on the four points farthermost from the wall ranged from one to five per cent. The one at $y/y_{\mathfrak{C}} = 0.07$ required 43 per cent correction and the one nearest the wall was nearly a static pressure measurement and no correction was applied.

A significant result of the comparison in Figure 35 is that the boundary layer equations appear to adequately describe the viscous region in a highly rarefied flow. For instance, the mean free path of the gas for these plenum chamber conditions is on the order of one-tenth of an inch for about the last half of the nozzle length. If a Knudsen layer is defined as ten mean free paths from the nozzle wall, the outer edge of the Knudsen layer would correspond to about $y/y_{\mathfrak{C}} = 0.1$. This distance is about 25 per cent of the total boundary layer thickness. Since velocity slip and temperature jump have not been taken into account, the agreement is surprisingly good.

A comparison of calculated and measured pitot pressures is given in Figure 36 for the Mach nine nozzle. The continuous measured pitot pressure distribution was obtained by connecting the pitot probe to a linear potentiometer which in turn was connected to an x-y plotter along with the signal from the pitot probe pressure transducer. Thus, it was possible to get a continuous trace for the pitot pressure as a function of position rather than discrete points. Some experimental pitot pressure data are given in Figure 37 which were taken from

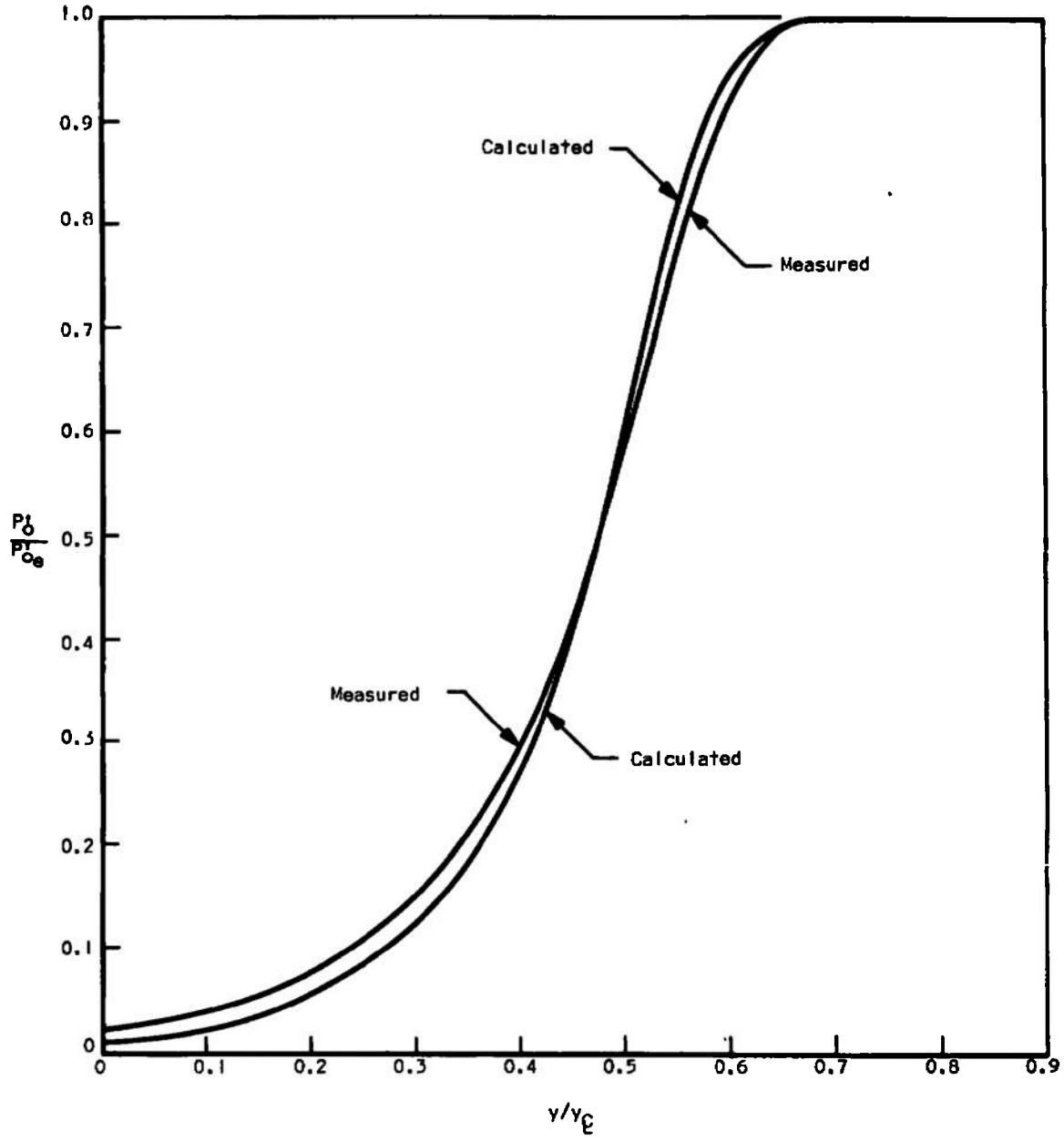

Fig. 36 Plot of Calculated and Measured Pitot Pressure Distributions at Exit of Mach Nine Nozzle

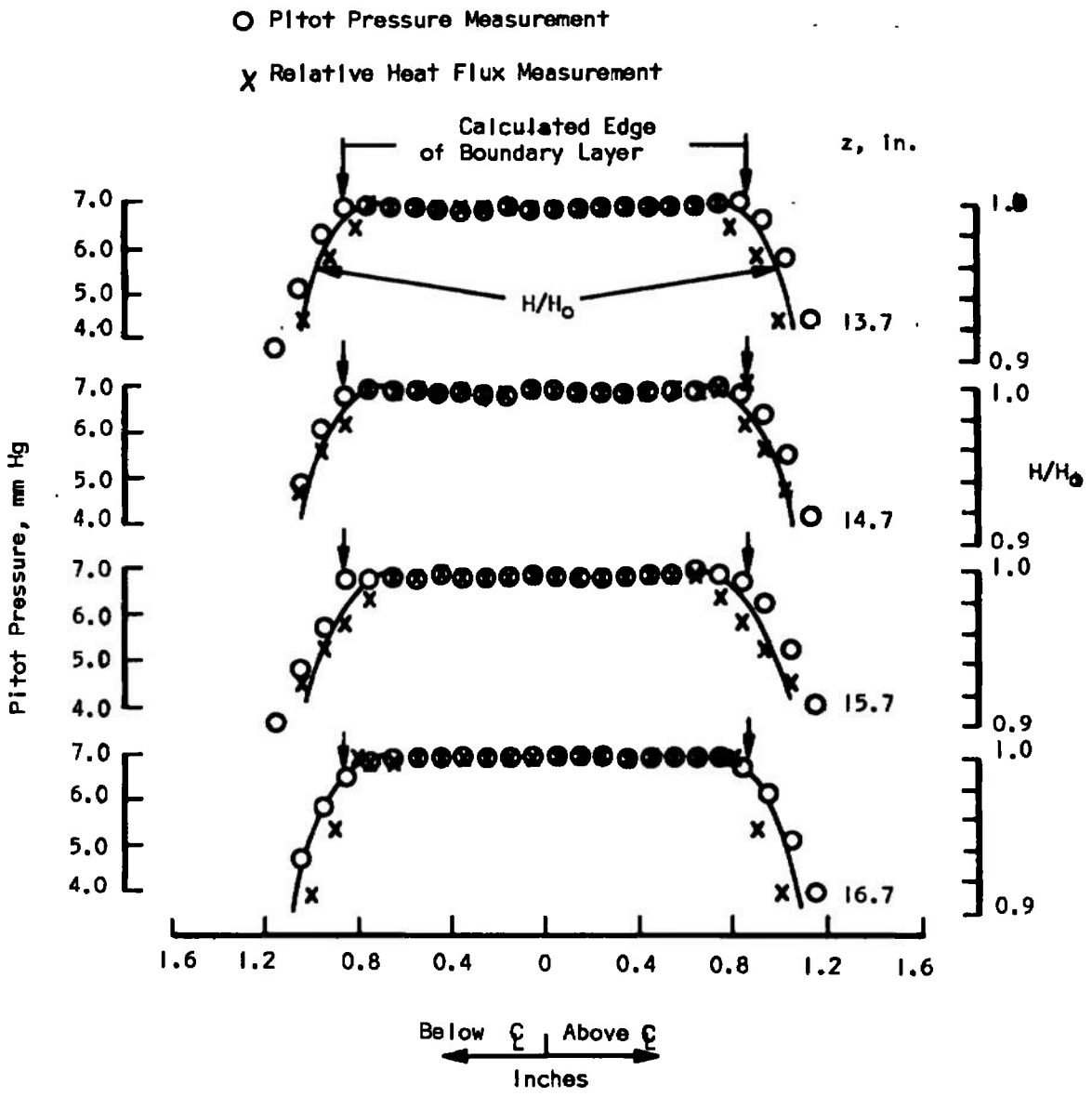

Fig. 37 Plot of Calculated Total Enthalpy Distribution, Calculated Edge of Boundary Layer, Measurements of Relative Heat Flux, and Measurements of Pitot Pressure for Mach Nine Nozzle

Reference 2. The previously mentioned method of taking pitot pressures was not available for use at the time these data were obtained.

The pitot pressure measurements presented in Figures 36 and 37 were not corrected for viscous effects since the correction required for the measurements over most of the boundary layer ranged from zero to two per cent. The region of the boundary layer near the wall in Figure 36 probably requires a significant correction, but good experimental data for viscous effects are not available for the flow conditions in this region, so a correction was not attempted. However, there are quantitative data available which indicate that any correction applied to the measured pitot pressures near the wall would lower the measured values and thus yield better agreement with the calculated distribution. Therefore, it must be concluded that this comparison between measured and calculated pitot pressures is rather good.

A pitot pressure survey such as that given in Figure 37 is usually the only information available for determining the boundary layer thickness. It is usually a good assumption to consider the pitot pressure distribution approximately the same as the velocity distribution near the edge of the boundary layer. There are situations, however, where this assumption is not justified. Examples of this are illustrated in Figures 21 through 24, pages 46 through 49. The pitot pressure is a function only of the Mach number at each axial location since the static pressure is assumed constant; therefore, the pitot pressure will drop off at the same point as the Mach number. For these cases one can see that a pitot survey would be very misleading as to the location of the

edge of the boundary layer since the Mach number is constant through much of the boundary layer. Fortunately, near the exit of supersonic and hypersonic nozzles where most of the total energy of the flow has been converted into velocity, the temperature distribution across the boundary layer is such that the Mach number, and hence the pitot pressure, is usually a good way to find the edge of the boundary layer. However, for subsonic flows, and supersonic flows where the static temperature is high relative to the wall temperature, the pitot pressure is not a good means for such an investigation.

The measured pitot pressures in Figure 37 were used to estimate δ for the Mach nine nozzle. The calculated values of δ are indicated for comparison with the measured pressures. For the conditions at the exit of this nozzle, the measured values of δ are consistent with the calculated values. Table II gives a tabulated comparison of the calculated and experimental values of Mach number and displacement thickness at the exit of the Mach three and nine nozzles. The actual displacement thickness was calculated using the actual Mach number and actual nozzle wall radius.

TABLE II
COMPARISON OF THEORY AND ACTUAL VALUES

	M		δ^*(inches)	
Nozzle	Experimental	Calculated	Experimental	Calculated
Mach Three	3.28	3.29	2.47	2.41
Mach Nine	9.30	9.27	0.95	0.96

Included in Figure 37 is a comparison between the relative heat flux measurements of Potter and Carden and the calculated distribution of H/H_o. The probe used to make these measurements is discussed briefly in Reference 2 and is said to measure about one-half the actual value of T_o. The discrepancy between the measured values of relative heat flux, that is, $T_o'/T_{o_{\ell}}'$, and calculated values of H/H_o ranged from zero to four per cent.

Heat transfer coefficients taken from Reference 11 are compared to calculated coefficients in Figure 38 for the Mach ten nozzle throat region. The heat transfer coefficient used in both the experiment and theory is defined by

$$\lambda = \frac{q_w}{T_{aw} - T_w} \tag{55}$$

where

$$\frac{T_{aw} - T_e}{T_o - T_e} = \sqrt{Pr} \tag{56}$$

Again there is consistent agreement between the experimental data and numerical solutions. In Reference 11, Carden has compared similar solutions with these experimental heat transfer rate measurements. The agreement is good especially downstream of the throat. However, the non-similar solutions presented herein predict the heat transfer rate at the throat more accurately than do the similar solutions. However, this would be expected since the conditions for similar solutions are more difficult to satisfy near the throat.

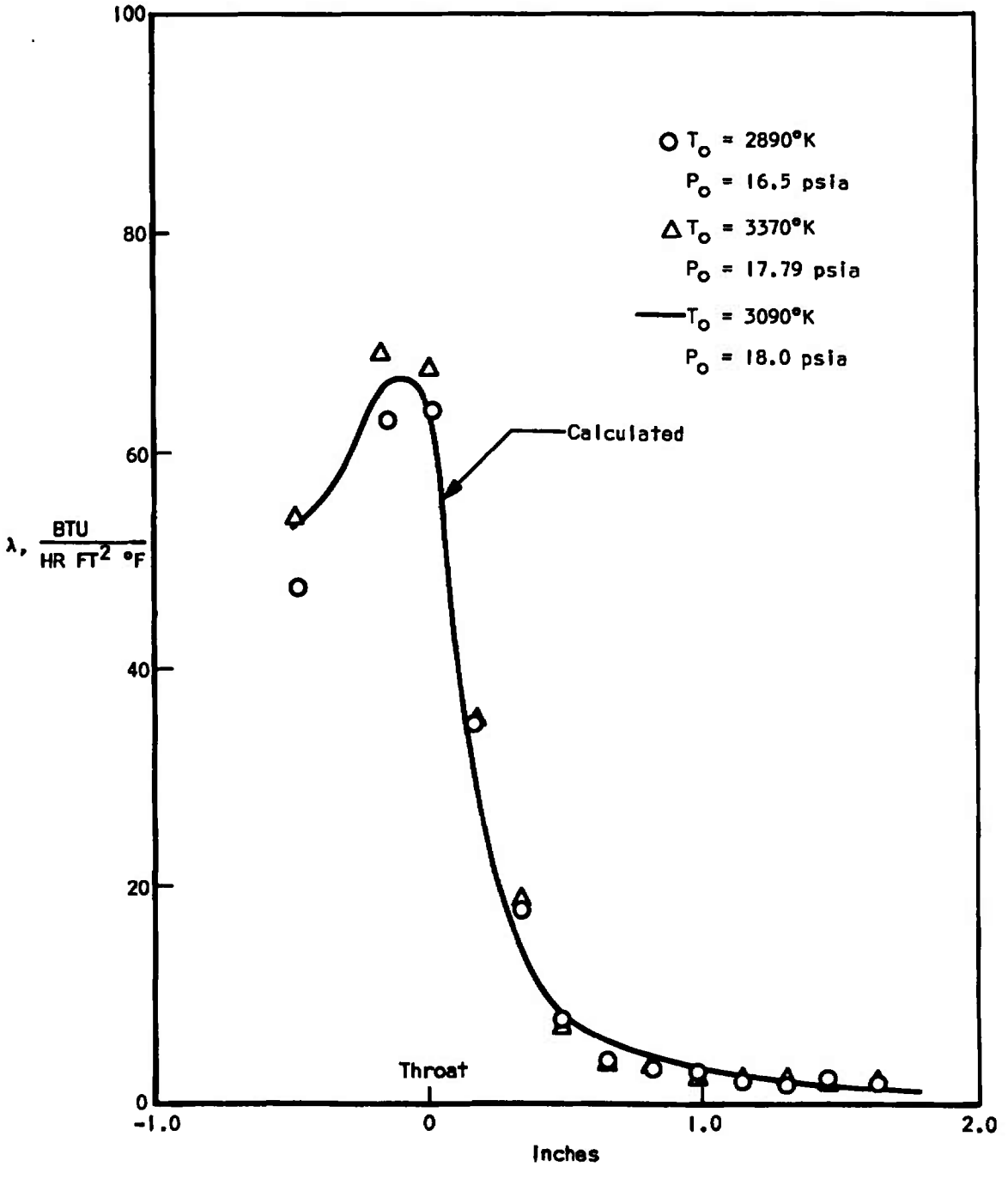

Fig. 38 Plot of Calculated and Measured Heat Transfer Coefficients in Mach Ten Nozzle

SECTION V
CONCLUSIONS

The axisymmetric laminar boundary layer equations including second-order transverse curvature terms have been adapted to the purpose of describing internal laminar boundary layers associated with axisymmetric nozzles. These equations have been formulated for solution similar to the method used by Jaffe, Lind, and Smith for the external boundary layer equations. This approach was taken in order to take maximum advantage of the numerical integration techniques which Jaffe, Lind, and Smith have developed.

Non-similar solutions were obtained for four existing low density nozzles using various wall temperature distributions. Appropriate solutions were compared to experimental data which were taken for the specific purpose of testing the theoretical results. Also comparisons were made with data that have been taken in the past by Potter and Carden. In all cases the theoretical solutions appeared to be in substantial agreement with the experimental data. Therefore, it is concluded that this set of equations, which is an approximation to the general form of the continuity equation, Navier-Stokes equations, and energy equation, adequately describes the viscous flow region in the low density axisymmetric nozzles considered.

Probably the most important result of the investigation is the capability to analyze the boundary layer in an existing or hypothetical

axisymmetric nozzle of arbitrary geometry, plenum chamber conditions, and wall temperature distribution. The satisfaction of such a need is both economical and practical.

The boundary layer equations have been shown to adequately predict physical phenomena in a gas that is highly rarefied. From this result it would seem appropriate to apply the boundary layer equations to the slip flow and temperature jump regime by properly modifying the wall boundary conditions.

Interesting and useful extensions of this work would be the following: (1) modify the transformation variables and/or the program to overcome the aforementioned difficulty near the nozzle centerline, (2) include velocity slip and temperature jump in the wall boundary conditions, (3) include the possibility of non-equilibrium, and (4) apply this non-similar method to the design of nozzles. Actually this latter extension would be rather simple, since the convergence of the solution could be accomplished by fixing the effective inviscid nozzle wall and iterating on the actual nozzle wall rather than vice versa as it is now done. In this case the input to the program for each successive iteration would be the actual nozzle wall radius calculated by the previous iteration. The properties along the centerline would of course be those for which the nozzle is intended to achieve. These properties are usually obtained from an inviscid method of characteristics solution by specifying the desired plenum chamber conditions, throat radius, maximum expansion angle, and uniform flow conditions at the nozzle exit.

BIBLIOGRAPHY

1. Potter, J. L. and J. A. Durand. "Analysis of Very Thick Laminar Boundary Layers in Axisymmetric High-Speed Fluid Flow," Development In Theoretical and Applied Mechanics, New York: Plenum Press, 1963, pp. 341-360.

2. Potter, J. L. and W. H. Carden. "Design of Axisymmetric Contoured Nozzles for Laminar Hypersonic Flow," AIAA Preprint No. 68-372, Presented at AIAA Third Aerodynamics Conference, San Francisco, California, April, 1968.

3. Cohen, C. B. and E. Reshotko. "The Compressible Laminar Boundary Layer with Heat Transfer and Arbitrary Pressure Gradient," NACA Report 1294, 1956.

4. Jaffe, N. A., R. C. Lind, and A. M. O. Smith. "Solution to the Binary Diffusion Laminar Boundary Layer Equations Including the Effect of Second-Order Transverse Curvature," AIAA Journal, Vol. 5, No. 9, 1967, pp. 1563-1569.

5. Probstein, R. F. and E. Elliott. "The Transverse Curvature Effect in Compressible Axially Symmetric Laminar Boundary-Layer Flow," Journal of the Aeronautical Sciences, Vol. 23, No. 3, 1956, pp. 208-222.

6. Illingworth, C. R. "Steady Flow in the Laminar Boundary Layer of a Gas," Royal Society of London Proceeding Series A, Vol. 199, 1949, pp. 533-558.

7. Levy, S. "Effect of Large Temperature Changes (Including Viscous Heating) Upon Laminar Boundary Layers with Variable Free-Stream Velocity," Journal of Aeronautical Sciences, Vol. 21, No. 7, 1954, pp. 459-474.

8. Olmsted, J. M. H. Real Variables. New York: Appleton-Century Crafts, Inc.

9. Adams, J. C., Jr. "Similar Solutions for Viscous Compressible Laminar Flow in Slender Axisymmetric Channels," Ph.D. dissertation, North Carolina State University, 1966.

10. Kinslow, M. and J. T. Miller. "Non-Equilibrium Expansion of a Diatomic Gas Through a Convergent-Divergent Nozzle," Physics of Fluids, Vol. 9, 1966, pp. 1703-1708.

11. Carden, W. H. "Local Heat-Transfer Coefficients in a Nozzle with High-Speed Laminar Flow," AIAA Journal, Vol. 3, No. 12, 1965, pp. 2183-2188.

UNCLASSIFIED

Security Classification

DOCUMENT CONTROL DATA - R & D

(Security classification of title, body of abstract and indexing annotation must be entered when the overall report is classified)

1. ORIGINATING ACTIVITY (Corporate author)	2a. REPORT SECURITY CLASSIFICATION
Arnold Engineering Development Center ARO, Inc., Operating Contractor Arnold Air Force Station, Tenn. 37389	UNCLASSIFIED
	2b. GROUP N/A

3 REPORT TITLE

THEORETICAL AND EXPERIMENTAL INVESTIGATION OF BOUNDARY LAYERS IN LOW DENSITY HYPERSONIC AXISYMMETRIC NOZZLES

4. DESCRIPTIVE NOTES (Type of report and inclusive dates)

Final Report September 1967 to January 1968

5 AUTHOR(S) (First name, middle initial, last name)

David L. Whitfield, ARO, Inc.

6 REPORT DATE	7a. TOTAL NO. OF PAGES	7b. NO OF REFS
September 1968	89	11

8a. CONTRACT OR GRANT NO	9a. ORIGINATOR'S REPORT NUMBER(S)
F40600-69-C-0001 b. PROJECT NO 7663 c. Task 766301 d Program Element 6240539F	AEDC-TR-68-193
	9b. OTHER REPORT NO(S) (Any other numbers that may be assigned this report) N/A

10 DISTRIBUTION STATEMENT

This document has been approved for public release and sale; its distribution is unlimited.

11 SUPPLEMENTARY NOTES	12 SPONSORING MILITARY ACTIVITY
Available in DDC.	Arnold Engineering Development Center (AETS) Arnold AF Station, Tenn. 37389

13 ABSTRACT

The viscous flow region in low density hypersonic axisymmetric nozzles was investigated both theoretically and experimentally. Non-similar solutions were obtained for the internal laminar boundary layer equations which include second-order transverse curvature terms. These solutions were obtained on a CDC 1604 digital computer. Four existing low density axisymmetric nozzles were considered. Numerical solutions were obtained for these nozzles using various plenum chamber conditions and wall temperature distributions. The plenum chamber conditions used in the numerical solutions for these nozzles produced a test section Mach number range of about 3.0 to 18.0 and a test section Reynolds number per foot range of about 1000 to 15,000. Some results of the numerical solutions are compared with experimental measurements of pitot pressure, relative heat flux, and nozzle wall heat transfer coefficients. In all comparisons the numerical solutions appear to be consistent with the experimental data.

DD FORM 1 NOV 65 1473

UNCLASSIFIED

Security Classification

14. KEY WORDS	LINK A		LINK B		LINK C	
	ROLE	WT	ROLE	WT	ROLE	WT
nonsimilar boundary layers						
hypersonic flow						
low density						
nozzles, axisymmetric, supersonic, hypersonic						